# EFFECT OF IR780-LOADED SILICA-COATED GOLD NANORODS FOR PHOTODYNAMIC THERAPY OF CANCER

by

**Merve Yünlü Doğruyol**

B.S., in Biomedical Engineering, İzmir Katip Çelebi University, 2019

Submitted to the Institute of Biomedical Engineering
in partial fulfillment of the requirements
for the degree of
Master of Science
in
Biomedical Engineering

Boğaziçi University
2023

# ACKNOWLEDGMENTS

I would like to thank Prof. Dr. Murat Gülsoy greatly for his crucial advice and suggestions in every respect throughout this study. I am appreciative to him for giving me this chance to write my master's thesis.

I am also grateful to Dr. Zeliha Cansu Canbek Özdil who supported and helped me to provide nanoparticle synthesis.

Thanks to my colleagues; Dr. Burcu Güleryüz, Dr. Melike Güney Akkurt, and Ayşe Işık for their help in the lab during my experiments and their friendships.

I would also like to thank my dearest husband and family members who have always been supportive and encouraged me in every respect.

# ACADEMIC ETHICS AND INTEGRITY STATEMENT

I, Merve Yünlü Doğruyol, hereby certify that I am aware of the Academic Ethics and Integrity Policy issued by the Council of Higher Education (YÖK) and I fully acknowledge all the consequences due to its violation by plagiarism or any other way.

Name :

Signature:

Date:

# ABSTRACT

## EFFECT OF IR780-LOADED SILICA-COATED GOLD NANORODS FOR PHOTODYNAMIC THERAPY OF CANCER

Photodynamic therapy (PDT) is a new approach to cancer treatment that activates a photosensitizer (PS), a light-sensitive chemical, with a specific wavelength of light. PDT is a promising new method, however, the efficacy of PDT is still limited because of a low accumulation of PS in the target cell and limited penetration of light to the deeper tissue which prevents the killing of all cancer cells. As a result, cancer recurrence is inevitable. Gold nanostructures are good biocompatible carriers of PS. Increasing PS accumulation on the target site leads to the effective destruction of cancer cells, but different cancer cells require different approaches. One of the resistant colon cancer types is HCT116 and it needs a better approach to treatment. Gold nanorods (GNRs) have a high absorption spectrum at near-infrared (NIR) as compared with other types of Gold nanoparticles (GNPs). However, GNRs are limited for the loading amount of PS and they tend to aggregate within cells. To overcome these limitations, we will develop mesoporous silica-coated GNRs ($GNRs@SiO_2$) for effective PS loading in this study. To test this hypothesis, we aim to test the PDT efficacy of IR780, as a PS, loaded $GNRs@SiO_2$, ($GNRs@SiO_2@IR780$) and $GNRs@SiO_2@PEG$ ($GNRs@SiO_2@IR780@PEG$). This investigation of PDT with $GNRs@SiO_2@IR780$ and $GNRs@SiO_2@IR780@PEG$ will cause a dramatic decrease in colon cancer volume as compared with $GNRs@SiO_2$ alone and $GNRs@SiO_2@PEG$ alone.

**Keywords:** Photodynamic Therapy, Colon Cancer Cells, Gold Nanorods, Silica Coating, IR780.

# ÖZET

## IR780 YÜKLÜ SİLİKA KAPLI ALTIN NANOÇUBUKLARIN KANSERİN FOTODİNAMİK TERAPİ ÜZERİNDEKİ ETKİSİ

Fotodinamik terapi (FDT), belirli bir dalga boyuna sahip ışık ile ışığa duyarlı bir kimyasal olan bir fotosensitizanı (FS) aktifleştirilmesidir. Ancak hedef hücrede düşük bir FS birikimi ve daha derin dokuya sınırlı ışık penetrasyonu nedeniyle FDT'nin etkinliği hala sınırlıdır. Sonuç olarak, kanserin tekrarlaması kaçınılmazdır. Altın nanoyapılar, FS için etkili biyouyumlu taşıyıcılardır. Hedef bölgede artan FS birikimi, kanser hücrelerinin etkili bir şekilde yok edilmesine yol açar, ancak farklı kanser hücreleri için farklı yaklaşımlar gerekebilir. Dirençli kolon kanseri türlerinden biri HCT116'dır ve tedavisi için daha etkili bir yaklaşım ihtiyacı vardır. Altın nanoçubuklar, diğer gold nanopartikül türlerine göre yakın-kızılötesi frekanslarında daha yüksek absorpsiyon spektrumuna sahiptir. Bununla birlikte, altın nanoçubukların FS yükleme potansiyeli zayıftır ve hücreler içinde agregasyon oluşturma eğilimindedirler. Bu sorunların üstesinden gelmek için, bu çalışmada etkili FS yüklemesi için mezo-gözenekli silika kaplı altın nanoçubuklar ($GNRs@SiO_2$) geliştireceğiz. Bu hipotezi test etmek için, fotonsensitizan olan IR780 yüklü $GNRs@SiO_2$ ($GNRs@SiO_2@IR780$) ve $GNRs@SiO_2@PEG$ ($GNRs@SiO_2@IR780@PEG$) parçacıklarının FDT etkinliğini test etmeyi amaçlıyoruz. IR780 yüklü parçacıklar ile yapılan bu FDT araştırması, tek başına $GNRs@SiO_2$ ve tek başına $GNRs@SiO_2@PEG$ ile karşılaştırıldığında kolon kanseri hacminde dramatik bir azalmaya neden olacaktır.

**Anahtar Sözcükler:** Fotodinamik Terapi, Kolon Kanseri Hücreleri, Altın Nanoçubuklar, Silika Kaplama, IR780

# TABLE OF CONTENTS

# LIST OF FIGURES

# LIST OF TABLES

# LIST OF SYMBOLS

| | |
|---|---|
| $M$ | Molar |
| $\mu M$ | Micromolar |
| $nm$ | Nanometer |
| $mL$ | Milliliter |
| $M\Omega.cm$ | Megaohm Centimeter |
| $\mu L$ | Microliter |
| $O$ | Oxygen |
| $^1O_2$ | Singlet Oxygen |
| $CO_2$ | Carbon Dioxide |
| $Si$ | Silicon |
| $Au$ | Gold |
| $gr$ | Gram |
| $g/mol$ | Gram per Mole |
| $^oC$ | Degrees Celsius |
| $C$ | Concentration |
| $g$ | g-force |
| $mg/mL$ | Milligram per Milliliter |
| $\mu g/mL$ | Microgram per Milliliter |
| $mm$ | Millimeter |
| $n$ | Number of Trials |
| $V$ | Volume |
| $cm$ | Centimeter |
| $mW/cm^2$ | Milliwatt per Square Centimeter |
| $J/cm^2$ | Joule per Square Centimeter |
| $mol/L$ | Mole per Liter |
| $\varepsilon$ | Molar Absorptivity |
| $b$ | Path Length |
| $HAuCl_4$ | Chloroauric Acid |

| | |
|---|---|
| $AgNO_3$ | Silver Nitrate |
| $NaBH_4$ | Sodium Borohydride |
| $NaOH$ | Sodium Hydroxide |
| $HCl$ | Hydrochloric Acid |
| $AA$ | L-ascorbic Acid |

# LIST OF ABBREVIATIONS

| | |
|---|---|
| ANOVA | Analysis of Variance |
| AR | Aspect Ratio |
| BSE | Backscattered Electrons |
| Ce6 | Chlorin e6 |
| CTAB | Cetyltrimethylammonium Bromide |
| C | Concentration |
| DI Water | Distilled Water |
| DMEM | Dulbecco's Modified Eagle Medium |
| DMSO | Dimethyl Sulfoxide |
| EE % | Encapsulation Efficiency |
| EDS | Energy Dispersive Spectrometry |
| FBS | Fetal Bovine Serum |
| FTIR | Fourier-Transform Infrared Spectroscopy |
| GNPs | Gold Nanoparticles |
| GNRs | Gold Nanorods |
| LED | Light-Emitting Diode |
| LSPR | Localized Surface Plasmon Resonance |
| L-SPR | Longitudinal Surface Plasmon Resonance |
| MTT | 3-[4,5-dimethylthiazol-2-yl]-2,5 diphenyl tetrazolium bromide |
| NIR | Near-Infrared |
| OD | Optical Density |
| PBS | Phosphate-buffered Saline |
| PEG | Polyethylene Glycol |
| PDT | Photodynamic Therapy |
| PS | Photosensitizer |
| PTT | Photothermal Therapy |
| ROS | Reactive Oxygen Species |
| SE | Secondary Electrons |

| | |
|---|---|
| SEM | Scanning Electron Microscopy |
| SPR | Surface Plasmon Resonance |
| STEM | Scanning Transmission Electron Microscopy |
| TEM | Transmission Electron Microscopy |
| TEOS | Tetraethyl Orthosilicate |
| T-SPR | Transverse Surface Plasmon Resonance |
| UP Water | Ultra-Pure Water |
| UV-VIS | Ultraviolet-Visible |

# 1. INTRODUCTION

## 1.1 Innovation

Different cancer cells require different approaches. One of the resistant colon cancer types is HCT116 and it needs a better approach to treatment [1]. The PDT application by using gold nanorods (GNRs) will enhance colon cancer therapy without any side effects. GNRs have absorption in the NIR spectrum and can efficiently generate heat from the incident light because of their high absorption ability. When we irradiate GNRs with a certain external light, the temperature of target cells will increase, and this photothermal therapy (PTT) activity provides destroying the cancer cells [2–4]. However, silica coating of gold nanorods increases the photothermal stability, therefore under lower fluences of laser light, $GNRs@SiO_2$ will not cause an increase of heat in the cells [2]. Thus, we will observe only the PDT activity of PS-loaded $GNRs@SiO_2$.

In this study, we will use 785 nm laser light to provide PDT by using IR780 as a PS through $GNRs@SiO_2$. At the same time, light can penetrate deeper tissue with this long wavelength. Thus, we will overcome the limitation of the penetration of light by using a 785 nm laser light source. The novelty of our study is using IR780 loaded $GNRs@SiO_2$ on HCT116 colon cancer cells under 785 nm laser light exposure.

PS should be accumulated in the target cells for PDT applications. Most photosensitizers are hydrophobic and due to possible interactions with cellular lipid components, we can get a better accumulation ability in tumors. However, photosensitizers should also circulate in the blood to reach the target cells. Thus, they should be at least partially water-soluble to disperse in the bloodstream [5]. In this study, we will use IR780 as a PS and it is one of the hydrophobic photosensitizers. It offers advantages with the ability of strong optical absorption in the NIR region, producing reactive oxygen species (ROS) and increasing cell temperature simultaneously under light exposure [6]. However, its hydrophobicity limits clinical applications because it

is hard to dissolve in water. To provide the water solubility of IR780, we will load it to the $GNRs@SiO_2$. At the same time, $GNRs@SiO_2$ provide high drug loading because of silica shells compared to uncoated GNRs [7]. In this way, the accumulation of IR780 on the target tumor site will increase and PDT activity will provide more destruction to the cancer cells. IR780 has an absorption peak at a 780 nm wavelength with a certain light intensity [6] and the as-prepared GNRs have a longitudinal surface plasmon resonance (SPR) peak at 785 nm. Therefore, we will use 785 nm red laser light to activate IR780 and $GNRs@SiO_2$ effectively. The novelty of our study is using IR780 for loading with $GNRs@SiO_2$ on HCT116 colon cancer cells under 785 nm laser light exposure.

IR780 loading has been assessed with different types of nanostructures for *in vitro* PDT and shown effective results but has not been tried to treat HCT116 cells by loading with $GNRs@SiO_2$ [8, 9].

The novelty of our study is the destruction of the HCT116 cancer cell line by using IR780 loaded $GNRs@SiO_2$ under 785 nm red light exposure to make active IR780 and to increase cancer cell death.

## 1.2 Approach

**Aim 1.** Test the PDT efficacy of $GNRs@SiO_2@IR780$.

IR780 is a near-infrared dye that has a specific absorption peak at 780 nm. We can overcome the penetration limitation by using IR780 as its peak interaction is at a long wavelength. IR780 can be used for PDT and PTT applications but due to its hydrophobicity and toxicity, further clinical applications are limited. To provide high water solubility, non-cytotoxicity, and good biocompatibility, we will load IR780 to silica-coated gold nanorods. We hypothesize that IR780-loaded silica-coated gold nanorods will devastate the tumor site effectively.

**Objective 1.1** Test the dark toxicity of $GNRs@SiO_2$ and $GNRs@SiO_2@IR780$.

**Experimental Approach.** HCT116 cells will seed in a 96-well plate and after 24 hours of incubation, the dark toxicity of $GNRs@SiO_2$ and $GNRs@SiO_2@IR780$ will be evaluated at different concentrations on HCT116 cells. The optimal doses of $GNRs@SiO_2$ and $GNRs@SiO_2@IR780$ will be determined as lower doses than those that produce toxic effects.

**Expected Results.** We expect that $GNRs@SiO_2$ and $GNRs@SiO_2@IR780$ are non-toxic without light irradiation. However, after a certain concentration, they may become toxic to the cells. We will test them at different concentrations to find the toxic dose. We will determine the optimal concentrations to be lower than the point where toxicity begins.

**Objective 1.2** Test only 785 nm laser light on HCT116 cells at different fluences (energy densities).

**Experimental Approach.** HCT116 cells will seed in a 96-well plate and after 24 hours of incubation, we will apply 785 nm laser light and test different energy densities to determine the optimum energy densities.

**Expected Results.** We expect that 785 nm light is non-toxic without any light-sensitive chemicals. However, after a certain energy density, 785 nm light may become toxic for the cells. We will test the laser light at different concentrations to find the toxic dose. We will determine the optimal energy densities to be lower than the point where toxicity begins

**Objective 1.3** Test the PDT activity of optimal doses of $GNRs@SiO_2$ and $GNRs@SiO_2@IR780$.

**Experimental Approach.** HCT116 cells will seed in a 96-well plate and after 24 hours of incubation, we will incubate the cells with optimal doses of $GNRs@SiO_2$

and $GNRs@SiO_2@IR780$ for 2 hours because the most effective accumulation of IR780-loaded nanoparticles occurs within 2 hours as specified in the literature. After the incubation, we will apply 785 nm laser light at optimal energy densities to activate $GNRs@SiO_2$ and $GNRs@SiO_2@IR780$.

**Expected Results.** We expect that $GNRs@SiO_2$ will not show the PDT effect due to a lack of PS. Since IR780 is loaded to $GNRs@SiO_2$ ($GNRs@SiO_2@IR780$), we will observe a remarkable cell death on HCT116 cells, under light exposure. We will determine the most effective doses of $GNRs@SiO_2$ and energy densities of 785 nm for the destruction of HCT116 cells.

**MTT Assay for Cell Viability and Proliferation.** The MTT (3-[4,5-dimethylthiazol-2-yl]-2,5 diphenyl tetrazolium bromide) assay is an assessment to detect cell proliferation and cytotoxicity, and quantification of cell viability. After all experimental approaches, 24 hours of incubation will follow the experiments, and then 10 $\mu L$ MTT solution will be added to each well for the assessment of cell viability. The media will be removed after 3 hours of incubation, and each well will receive 100 $\mu L$ Dimethyl Sulfoxide (DMSO). Then, the plate will be put on the shaker for 5 minutes and placed in the optical reader device. Statistical analysis will be performed by using IBM SPSS Statistics.

# 2. BACKGROUND

## 2.1 Photodynamic Therapy for Cancer

Photodynamic therapy (PDT) is a promising method for destroying malignancies with the use of a photosensitizer (PS), a light-sensitive reagent, and a specified wavelength of light [10, 11]. In PDT, the PS is stimulated to excited energy levels by the light of the specific wavelength (Figure 2.1). Then, this excited PS returns to the ground state by transferring its excess energy to nearby molecular oxygens. Reactive oxygen species (ROS) such as free radicals (hydroxyl radicals, hydrogen peroxide, and superoxide anion) or singlet oxygen ($^1O_2$) are formed in this mechanism. Especially, since singlet oxygen is highly cytotoxic for the cells, singlet oxygen generation is the most important ROS generation mechanism for PDT applications [10, 12–14].

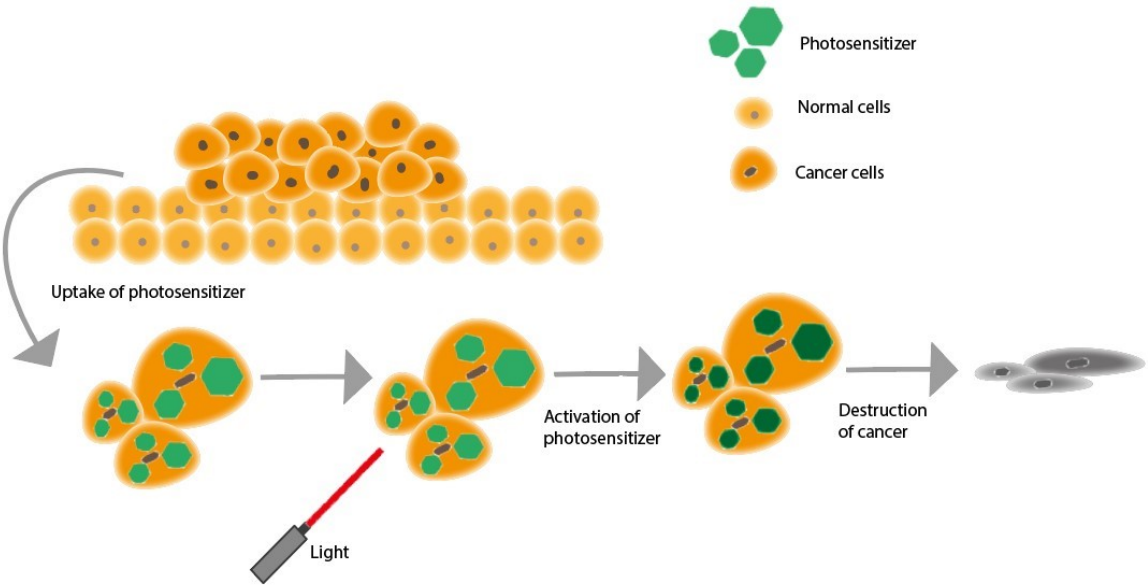


**Figure 2.1** The specific wavelength of light and photosensitizer interaction is the basis of photodynamic treatment.

The traditional therapeutic methods for cancer treatments include surgery, radiation, and chemotherapy may cause some serious side effects [15]. Immunological changes, inflammation, and tissue damage are all possible negative side effects of can-

cer surgery [16]. Fatigue, loss of taste, and hair loss can occur during radiotherapy [17]. Chemotherapy has several negative complications including fatigue and weakness, nausea and vomiting, and hair and weight loss [18]. Researchers are looking toward newer and more innovative cancer treatments to minimize these adverse consequences. PDT is a promising new technique since it avoids the negative impacts of traditional methods.

However, the efficacy of PDT is still limited because of a low accumulation of PS in the target cell and limited penetration of light to the deeper tissue. These limitations prevent the complete removal of cancer and as a result, cancer recurrence is inevitable [19–21]. Different strategies have been assessed to increase the efficacy of PDT, such as targeted delivery of the photosensitizers [22], uploading photosensitizers in nanostructure [23, 24], or combining PTT with PDT [25–29]. Gold nanostructures are promising good biocompatible carriers of PS. When gold nanostructures are combined with PS, the reaction to cancer tissue is more focused than when PS is used alone. Increasing the PS accumulation on the target site leads to the effective destruction of cancer cells [21, 25–30].

PDT by using gold nanostructures can be applied to different cancer cell types. HCT116 is a resistant colon cancer type, and it needs a better approach to treatment. Therefore, the improvement of PDT and enhancement of cancer cell death would be valuable for the treatment of HCT116 colon cancer cells.

## 2.2 Gold Nanostructures for PDT of Cancer

Gold nanostructures are good biocompatible carriers and since they have special chemical and physical characteristics, they exhibit high surface activity [31, 32]. The enhanced permeability and retention (EPR) mechanism allow gold nanostructures containing PS to cumulate in the tumor site more effectively, so the effectiveness of killing cancer cells increases when exposed to light [33]. For the therapy of cancer, many types of gold nanostructures, such as spherical gold nanoparticles, gold nanorods,

and gold nanoclusters, are being investigated [34]. Under illumination, spherical gold nanoparticles and gold nanorods tend to demonstrate localized surface plasmon resonance (LSPR), which is a consequence of free electron oscillations. Gold nanospheres and nanorods have an optical absorption spectrum ranging between visible and NIR [34, 35], making them promising agents to increase PDT activity [30]. A key characteristic of PDT when using PS is the production of ROS, which is enhanced by gold nanostructures in addition to the accumulation of PS [36, 37].

Xu et al. [38] examined the efficiency of ALA as a PS and its conjugation with GNPs in PDT by using three different kinds of light-emitting diode arrays with central wavelengths of 399, 502, and 621 nm and a mercury lamp with a central wavelength of 395 nm. The research group observed the intracellular PpIX levels in K562 cells and the singlet oxygen production of PpIX during irradiation. The 2 mM ALA-GNP conjugates were more cytotoxic to K562 cells than ALA by itself. Under green LED irradiation, ALA-GNPs conjugation provides effective K562 cell death when compared to the results of irradiation by a mercury lamp. These outcomes could be explained by GNPs' ability to increase the singlet oxygen output of PpIX.

Indocyanine green (ICG), a PS, and chitosan hybrid nanospheres (CSAuNR-ICG NSs) were successfully produced by Chen et al. [39] used for PTT-PDT combined therapy by using an 808 nm laser. ICG may be loaded effectively and protected against rapid hydrolysis by the chitosan matrix in the form of a sphere. ICG and AuNR were found to be capable of being delivered to the tumor site with high concentrations. CSAuNR-ICG NSs produced hyperthermia and sufficient ROS to kill target cancer cells completely when exposed to an 808 nm laser. The combined therapy greatly outperformed either PTT or PDT on its own in terms of synergy and therapeutic efficacy.

Meyers et al. [40] investigated a novel strategy for delivering PDT drugs. In this study, Silicon Phthalocyanine (Pc 4), as a PS, was used for targeted drug delivery by using epidermal growth factor peptide-targeted Au NPs (EGFpep-Au NPs). This *in vitro* study of PDT showed that EGFpep-Au NP-Pc 4 is two times more effective

at killing brain cancer cells than free Pc 4. Additionally, *in vivo* research, showed that using EGFpep-Au NP-Pc 4 enhances Pc 4 fluorescence accumulation in targeted tumors when compared to untargeted Au NPs. This study showed that EGFpep-Au NP-Pc 4 utilizes cancer-specific biomarkers to improve drug delivery and therapeutic effects in contrast to untargeted drug delivery.

According to studies, multifunctional nanoparticle systems mediated by gold nanostructures have advanced significantly and these applications are expected to increase the effectiveness of cancer treatment. However, before the clinical studies, these applications must overcome the limitations of the biodegradability of gold nanostructures.

## 2.3 Silica Coated Gold Nanostructures for PDT of Cancer

Gold nanostructures are promising nanoparticles for many light-based diagnostic and treatment approaches with an LSPR maximum in the range of 650 to 950 nm [41]. However, some of the gold nanostructures especially have two disadvantages as a theranostic approach: the number of theranostic agents that can be loaded is limited by the surface area's comparatively low specific area, and because the different shapes of gold nanostructures, frequently cluster and aggregate within cells [7, 42]. Many research groups are working to develop silica-coated gold nanostructure as a new theranostic system for tumor treatment to overcome these two disadvantages. Especially, mesoporous silica′s enormous specific surface area ensures a high pharmacological payload. As a result, the $Au@SiO_2$ is a promising and adaptable theranostic system, and this suggests possible *in vivo* applications [7, 43, 44].

Zhang et al. [7] showed that mesoporous silica-coated gold nanorods ($Au@SiO_2$) can be used to create a potential and flexible therapeutic and diagnostic platform for cancer. When loaded with doxorubicin hydrochloride, $Au@SiO_2 - DOX$ exhibits laser-triggered chemotherapeutic drug release and laser-induced hyperthermia. These therapeutic effects have the potential to be used in *in vivo* applications.

Seo et al. [43] developed methylene blue-loaded silica-coated gold nanorods ($MB-GNR@SiO_2$) core-shell nanoparticles for cancer imaging and PTT/PDT combined therapy. Compared to free GNRs or MB treatment, the cancer cell-killing ability was considerably higher when using $MB-GNR@SiO_2$ nanocomposites that provided a photon-induced dual modality of photothermal and photosensitizing effects simultaneously.

Huang et al. [45] designed a gold nanocluster coated with silica and conjugated to chlorin e6 (Ce6) PS ($AuNCs@SiO_2-Ce6$) for PDT guided by fluorescence imaging. The characteristics of the $AuNCs@SiO_2-Ce6$ are a high loading of Ce6, no undesirable release of Ce6 during circulation, effective cellular uptake of Ce6, which provides noticeably increased PDT efficacy compared to free Ce6, and fluorescence imaging-guided PDT. This designed nanoparticle provides a biocompatible, water-soluble, and stable system for PDT applications.

As shown in these studies, there are several advantages of silica coating. Silica is very stable; therefore, silica coating protects the fluorescent gold nanostructures by enhancing their chemical stability and photostability [46–48]. Silica may easily have several functional groups added to its surface [45, 46] so silica coating provides effective drug loading [49]. With all that, since silica coating prevents some acute damage from the laser-converted heat, it provides great potential for controlled PDT applications [7].

## 2.4 IR780 Loaded Silica Coated Gold Nanostructures for PDT of Cancer

The NIR dye IR780 iodide is more recent than the other conventional dyes. IR780 has high fluorescence intensity and the capacity to produce singlet oxygen under NIR radiation [49–51]. Thanks to these properties, IR780 dye has recently been used for PDT applications, effectively. IR780 can also be used as a PTT agent be-

cause it generates heat when exposed to light [49]. Despite the potential, the low tumor-targeting effectiveness and poor water solubility in water of IR780 iodide cause limitations for its usage in clinical applications [51]. Many studies have been made to improve the solubility and biocompatibility of IR780 to overcome its limitations [52].

Zhan et al. [52] created the brand-new IR780-encapsulating silica cross-linked micellar core-shell nanoparticles (NIR-Silica NPs) and they reported its use in *in vivo* biomedical imaging. The solubility and fluorescence intensity of NIR-Silica NPs is significantly higher than free IR780. But more crucially, the EPR effect of NIR-Silica NPs is very high because the NPs are very small (25 nm) and colloidal stable. Further testing using *in vitro* cell viability experiments revealed that NIR-Silica NPs are safe even at the even at concentration of 1.0 mg/mL which is very high. Long-term tumor imaging *in vivo* and sentinel lymph node mapping demonstrated that the NIR-Silica NPs have a high circulation duration and a great signal-to-noise ratio at a very low dye concentration.

Gonçalves et al. [53] assessed the PTT and PDT capabilities of IR780 when the gold core silica shell (AuMSS) nanorods were coupled for the first time. Excellent physicochemical characteristics of AuMSS nanorods enable their use as PTT and drug delivery agents. In this study, PEG-CH3 and gelatin (GEL) were employed to dual-functionalize AuMSS nanorods to enhance the colloidal stability and uptake by HeLa cancer cells. According to the data, adding IR780 (65 g per mg of AuMSS) boosts the PTT efficacy of AuMSS nanorods. Additionally, compared to the control, the absorption of the IR780-loaded AuMSS/T-PEG-CH3/T-GEL was around two times higher in HeLa cells.

Xia et al. [54] reported that a simple method of making targeted dual-modal photoacoustic (PA)/near-infrared (NIR) fluorescence imaging and better PTT/PDT for lung cancer by creating gold nanostars (GNSs) connected with matrix metallo-proteinases (MMP2) polypeptides (Ac-GPLGIAGQ) and IR780 iodide through bovine serum albumin (BSA). The targeting ligand was MMP2 polypeptides, the NIR fluo-rescence imaging and PTT/PDT agents were IR780 iodide, and the PA imaging and

PTT functions were performed by GNS, the IR780 molecule carrier. The stable and biocompatible nanoprobes ($GNS@BSA/I-MMP2$) were successfully accumulated on A549 cancer cells and demonstrated outstanding anticancer activity. Additionally, $GNS@BSA/I-MMP2$ NPs were able to show high specificity and effectively inhibit tumor growth. These NPs' anticancer effects NPs' anticancer effects improved the PDT/PTT combined applications based on IR780 and GNSs. These results suggest that $GNS@BSA/I-MMP2$ NPs may be used as a targeted PA/NIR probe for combination therapy and tumor diagnosis under single irradiation.

Since IR780 has poor aqueous media stability, rapid clearance, low water solubility, and toxicity at high dosages, its therapeutic use is limited [55, 56]. According to the literature, IR780 has been loaded into various nanostructures, which have enhanced its pharmacokinetics and pharmacodynamics characteristics. Notably, the majority of research used IR780 as a tracer agent physically enclosed in nanostructures without providing a thorough illustration of the stability of IR780 loading [56–58].

## 2.5 Anticancer PDT Studies on HCT116

One of the major cancer-related fatalities in the world is colon (colorectal) cancer [59]. Similar to many other solid tumors, this colorectal tumor's mortality is more often caused by metastases than by the primary tumor. The multi−step process of metastasis involves changing interactions between the extracellular matrix, enhanced cellular migration and motility, cellular extravasation, and the loss of the ability of cells to sustain growth [60–62]. The molecular mechanisms underlying this multi-step process still require a great deal of study [60, 63].

Many researchers investigated the antitumor therapeutic efficacy of human colon adenocarcinoma cells (HCT116 cells) considering the significance of the PS and nanostructures [64]. Tanaka et al. [65] reported that glucose consumption is higher in cancer cells than in healthy cells. In this research, the performance of PDT with a novel PS, Talaporfin, a drug utilized in clinical applications in Japan, was compared with chlorin

glycoconjugate (H2TFPC-SGlc). After colon cancer cells (HT29 and HCT116) and gastric cancer cells (MKN28 and MKN45) were incubated with PS and irradiated by using LED (Light Emitting Diode) light, cell death was compared. They evaluated the antitumor effects and accumulation and they reported that H2TFPC-SGlc was 30 times more cytotoxic *in vitro* than Talaporfin to cancer cells. The H2TFPC-SGlc *in vivo* accumulation in tumors was greater and tumor growth was dramatically slowed compared with Talaporfin. The experiments showed that this brand-new chlorin glycoconjugate is beneficial in anticancer PDT application on HCT116.

The cytotoxicity of several treatment groups on human colon cancer HCT116 cells was assessed by Chu et al. [66]. The development of ROS-responsive camptothecin (CPT) prodrug delivery system (MPEG-(TK-CPT)-PPa) allows for the simultaneous conjugation of CPT and the photosensitizer pyropheophorbide-a (PPa) to the same poly(ethylene glycol) methyl ether (MPEG) via a ROS-responsive thioketal (TK) and lipid linkage. Nanoparticles (NPs) (43.6 $\pm$ 0.8 nm) of the synthesized MPEG-(TK-CPT)-PPa conjugate self-assemble in solution. The covalently attached prodrug synchronizes the *in vivo* distribution of the two medicines and stops drug leakage during systemic circulation. This study showed that PPa-induced PDT and CPT-mediated chemotherapy result in the combined and improved inhibition of HCT116 tumor development.

Ballestri et al. [67] synthesized a new, non-symmetrical diaryl-porphyrin that was appropriately modified with a polymerizable pendant and used to create core-shell poly-methyl methacrylate nanoparticles ($PMMA@PorVa$). The particles, which were created using two distinct porphyrin loadings, have a small hydrodynamic diameter of about 70 nm, a positive zeta potential, and are spherical. Both the human ovarian adenocarcinoma cell line SKOV3 and the human colon cancer cell line HCT116 were used to investigate their phototoxicity. *In vitro* effectiveness and PDT activity of PS can both be preserved by covalently attaching PS to PMMA nanoparticles. Similar to free porphyrin, $PMMA@PorVa$ was able to prevent the proliferation of SKOV3 and HCT116 tumor cells.

# 3. MATERIALS AND METHOD

## 3.1 GNRs Synthesis

In this study, we synthesized GNRs by using the seed-mediated method described by Nikoobakht and El-Sayed including seed and growth solution preparation [68]. We produced monodispersed GNRs in a water solution with the properties of high yield and high aspect ratio [69].

### 3.1.1 Materials and Instrumentation

Cetyltrimethylammonium bromide (CTAB 99%), chloroauric acid ($HAuCl_4$, extra pure), silver nitrate ($AgNO_3$, extra pure), sodium borohydride ($NaBH_4$ 98%), Hydrochloric Acid (HCl), and L-ascorbic acid (AA) were received from Sigma Aldrich. The synthesis was done by using Ultra-Pure Water (UP Water) with a resistivity of 18.2 MΩ.cm.

It is important to keep the glassware clean by washing them with distilled water (DI Water). Additionally, the hot plate stirrer was used for synthesis.

### 3.1.2 Preparation of Chemical Substances

We prepared the chemical substances we need for GNR synthesis at the concentrations and volumes indicated in Table 3.1. The seed and growth solutions are prepared separately and in the next step, the seed solution is mixed with the growth solution to produce GNRs with the desired properties. Amounts are set for high volume. Synthesis can be made using the same ratios in desired volumes.

**Table 3.1**

The seed and growth solution is prepared using the chemical substances at the given concentration and volume.

| Chemical Substances | | | | | |
|---|---|---|---|---|---|
| Chemicals | Situation | Solution Conc. (M) | Volume (mL) | Molecular Weight (g/mol) | Molar Mass (gr) |
| CTAB | Stock | 0.1 | 500 | 364.45 | 18.2225 |
| $HAuCl_4$ | Stock | 0.10156 | 25 | 393.83 | 0.99993437 |
| $NaBH_4$ | Fresh | 0.026 | 40 | 37.83 | 0.0393432 |
| $AgNO_3$ | Fresh | 0.01 | 10 | 169.87 | 0.016987 |
| AA | Fresh | 0.1 | 10 | 176.12 | 0.17612 |
| HCl (5 M, 10 mL) | Fresh | 12 | 4.16 | - | - |

### 3.1.3 Preparation of CTAB capped Seeds

Briefly, the nanoparticles were created in high volume by adding freshly made, ice-cold $NaBH_4$ solution (1 mL, 0.0264 M) to a mixture of CTAB (47 mL, 0.1 M) and $HAuCl_4$ (0.1 mL, 0.1 M). After that, as shown in Figure 3.1, the mixture was vigorously stirred at 28 $^oC$ for 2 minutes with the cover closed to prevent evaporation. After being prepared for an hour, the solution with a light brown color can be used.

**Figure 3.1** Seed solution was prepared by using a hot plate stirrer with the stock solutions of CTAB and $HAuCl_4$ and fresh solution of $NaBH_4$.

The chemical substances for seed preparation were calculated corresponding to final concentrations as shown in Table 3.2.

**Table 3.2**

The chemical substances are used at the given stock concentration (M) and volume (mL) to prepare the seed solution.

| Seed Preparation | | | | | |
|---|---|---|---|---|---|
| Chemicals | Situation | Solution Conc. (M) | Volume (mL) | Molecular Weight (g/mol) | Molar Mass (gr) |
| CTAB | Stock | 0.1 | 500 | 364.45 | 18.2225 |
| $HAuCl_4$ | Stock | 0.10156 | 25 | 393.83 | 0.99993437 |
| $NaBH_4$ | Fresh | 0.026 | 40 | 37.83 | 0.0393432 |
| $AgNO_3$ | Fresh | 0.01 | 10 | 169.87 | 0.016987 |
| AA | Fresh | 0.1 | 10 | 176.12 | 0.17612 |
| HCl (5 M, 10 mL) | Fresh | 12 | 4.16 | - | - |

### 3.1.4 Preparation of Growth Solution

After seed preparation, the seeds must be included in the growth solution to obtain the desired size and rod-shaped particles in a controlled manner. We prepared the growth solution by adding $HAuCl_4$ (0.1 M, 1.26 mL) to CTAB (0.1 M, 250 mL) under stirring. After that, AA (0.1 M, 1.92 mL) was added quickly to the solution. The solution color is expected to turn from yellow to white at this stage. After color change, $AgNO_3$ (0.01 M, 3.59 mL) and HCl (5 M, 50 $\mu L$) solutions were added while the mixture was stirred. Finally, as shown in Figure 3.2, the 1.5 mL seed solution that we prepared before is added to the mixture quickly. After these stages are finished, the solutions are mixed for another 15 seconds and stored overnight at 28 $^oC$ in a water bath. Thus, the desired growth is completed.

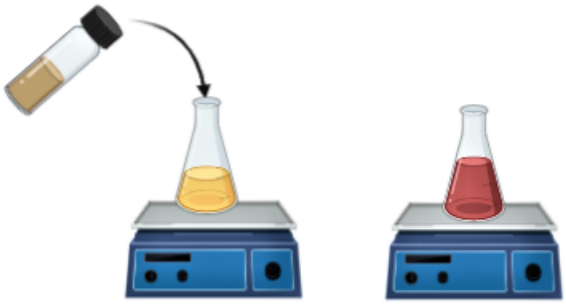

**Figure 3.2** The color change is seen after the seed solution has been added to the growth solution produced for the synthesis of GNRs at 28 $^oC$.

The chemical substances for the growth solution were calculated corresponding to final concentrations as shown in Table 3.3.

**Table 3.3**

The chemical substances are used at the given stock concentration (M) and volume (mL) to prepare the growth solution.

| Growth Solution Preparation | | | |
|---|---|---|---|
| Chemicals | Solution Conc. (M) | Volume (mL) | $C_Final$ (M) |
| CTAB | 0.1 | 250 | 0.1 |
| $HAuCl_4$ | 0.10156 | 1.264203919 | 0.0005 |
| $AgNO_3$ | 0.01 | 3.5949914 | 0.00014 |
| AA | 0.1 | 1.92588825 | 0.00075 |
| HCl | 5 | 0.005 | - |

## 3.2 $GNRs@SiO_2$ Synthesis

The produced GNRs with a localized surface plasmon resonance (LSPR) maximum in the 650 to 950 nm range provide a potential theranostic development for the treatment of cancer. However, due to their low specific surface area, GNRs can only carry a certain quantity of drugs. Also, since the GNRs frequently cluster and aggregate within cells, deep tissue penetration is lost when the desired NIR window is shifted to the visible spectral region. The mesoporous silica's enormous specific surface area ensures a high drug loading, therefore we created mesoporous silica-coated

gold nanorods ($GNRs@SiO_2$) as a new cancer theranostic system to overcome these limitations [7].

### 3.2.1 Materials and Instrumentation

Sodium hydroxide (NaOH, Isolab), Tetraethyl orthosilicate (TEOS, $\geq$ 99%, Sigma Aldrich), and ethanol (absolute, reag. 99.8 %, Merck) were used for silica coating. The synthesis was done by using UP water with a resistivity of 18.2 $M\Omega.cm$.

It is important to keep the glassware clean by washing them with distilled water (DI Water). Additionally, the stirrer, centrifuge, and centrifuge tubes (2 mL) were used for synthesis.

### 3.2.2 Preparation of $GNRs@SiO_2$

$GNRs@SiO_2$ were synthesized by using a previously published methodology with some changes [7, 70]. To eliminate excess CTAB, the synthesized GNRs were centrifuged at 8440 g for 40 minutes and twice washed with UP water. After that, 200 $\mu L$ of 0.1 M NaOH solution (diluted from 2 M NaOH, 0.1 gr pellet, and 1.2 mL DI water) was added to 20 mL purified GNRs while stirring. Then, three times at intervals of 30 minutes, 60 $\mu L$ of 20% TEOS in ethanol was added while being gently stirred. At 26—28$^oC$, the mixture was reacted for three days and after this step, $GNRs@SiO_2$ were thoroughly washed after being centrifuged at 8440 g for 40 minutes with ethanol or UP water according to application. The color change was slightly observed as shown in Figure 3.3 when compared with GNRs.

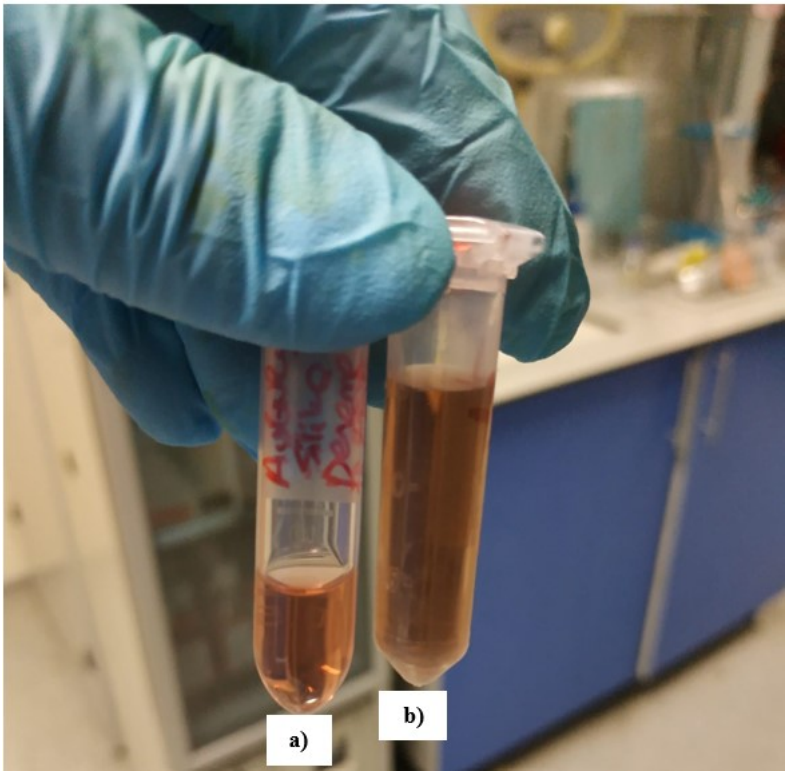


**Figure 3.3** a) $GNRs@SiO_2$ and b) GNRs solutions were compared, and the color change was slightly observed.

## 3.3 $GNRs@SiO_2@PEG$ Synthesis

Polyethylene glycol (PEG) is frequently used to coat $SiO_2$ nanoparticles (NPs) to reduce the coverage of exposed silanol groups, promote biocompatibility by limiting non-specific protein adsorption, and allow for greater electrolyte dispersion, such as that found in biological structures [71–73].

### 3.3.1 Materials and Instrumentation

PEG was received from Merck. The synthesis was done by using UP water with a resistivity of 18.2 $M\Omega.cm$.

It is important to keep the glassware clean by washing them with DI Water. Additionally, the stirrer, incubator/oven, centrifuge, and centrifuge tubes (2 mL) were

used for synthesis.

### 3.3.2 Preparation of $GNRs@SiO_2@PEG$

The synthesized $GNRs@SiO_2$ nanoparticles were dried overnight in an oven set to 80 $^oC$ and the amount of $GNRs@SiO_2$ was determined to be approximately 5.3 mg. Then, for the PEGylation, coating the surface of nanoparticles with PEG, 5.3 mg $GNRs@SiO_2$ were dispersed in 7.066 mL UP water and 0.01696 gr PEG pellet was dissolved in the solution overnight while stirring. After stirring, the $GNRs@SiO_2@PEG$ were split into 2 mL tubes, then centrifuged at 8440 g for 40 minutes, and washed with UP water several times.

## 3.4 $GNRs@SiO_2@IR780$ Synthesis

IR780 was used as a PS to show the photo-theranostic approaches of $GNRs@SiO_2$. IR780, a PS with considerable optical absorption and emission in the NIR range, is increasingly gaining attention from scientists working on cancer imaging and treatment. IR780 can create ROS and raise body temperature when exposed to NIR light, therefore it is a promising agent for use in cancer PDT and PTT applications. On the other hand, IR780 has poor water solubility, quick elimination, acute toxicity, and low tumor absorption, IR780 has been loaded and delivered to tumor cells utilizing a variety of nanoplatforms to get over these limitations. In this study, we focus on the IR780-loaded $GNRs@SiO_2$ that can be more efficient for increasing PDT cell-killing efficiency compared to IR780 alone.

### 3.4.1 Materials and Instrumentation

IR780 iodide (Dye content $\geq$ 95%) and ethanol (absolute, reag. 99.8 %) were used for PS-loading. The synthesis was done by using UP water with a resistivity of

18.2 $M\Omega.cm$.

It is important to keep the glassware clean by washing them with DI Water. Additionally, the stirrer, centrifuge, and centrifuge tubes (2 mL) were used for synthesis.

### 3.4.2 Preparation of $GNRs@SiO_2@IR780$

The synthesized $GNRs@SiO_2$ nanoparticles were dried overnight in an oven set to 80 $^oC$ and the amount of $GNRs@SiO_2$ was determined to be approximately 5.3 mg. Then, for the IR780 loading, 5.3 mg $GNRs@SiO_2$ were dispersed in 7.066 mL ethanol. Under gentle stirring, 2.304 mL IR780 (1 mg/mL) solution in ethanol was added to the $GNRs@SiO_2$ at dark. After overnight stirring, the $GNRs@SiO_2@IR780$ were split into 2 mL tubes, then centrifuged at 8440 g for 40 minutes, and washed with UP water several times.

## 3.5 $GNRs@SiO_2@IR780@PEG$ Synthesis

Many kinds of research studies on the different forms including polymeric, metallic, and PEG lipids for produced PS-loaded nanoparticles to overcome the limitations [74–76]. By protecting the PSs from the hostile environment of the body, these nanoplatforms can deliver them to the malignant location in a safe manner [76].

### 3.5.1 Materials and Instrumentation

PEG was received from Merck. The synthesis was done by using UP water with a resistivity of 18.2 $M\Omega.cm$.

It is important to keep the glassware clean by washing them with DI Water. Additionally, the stirrer, centrifuge, and centrifuge tubes (2 mL) were used for synthesis.

### 3.5.2 Preparation of $GNRs@SiO_2@IR780@PEG$

After centrifugation and washing, the synthesized $GNRs@SiO_2@IR780$ (5.3 mg) was dissolved in 7.066 mL UP water. Then, for the PEGylation, a 0.01696 gr PEG pellet was dissolved in the $GNRs@SiO_2@IR780$ solution overnight while stirring at dark. After stirring, the $GNRs@SiO_2@IR780@PEG$ were split into 2 mL tubes, then centrifuged at 8440 g for 40 minutes, and washed with UP water several times.

## 3.6 Characterization of Nanoparticles

The purpose of this section is to present the characterization of the synthesized nanostructure, $GNRs@SiO_2@IR780@PEG$. The synthesis process is shown briefly in Figure 3.4. Firstly, GNRs are coated with mesoporous silica, then IR780 PS is loaded into the nanostructure. Lastly, to prevent leakage of PS and provide stability, $GNRs@SiO_2@IR780$ is coated with PEG.

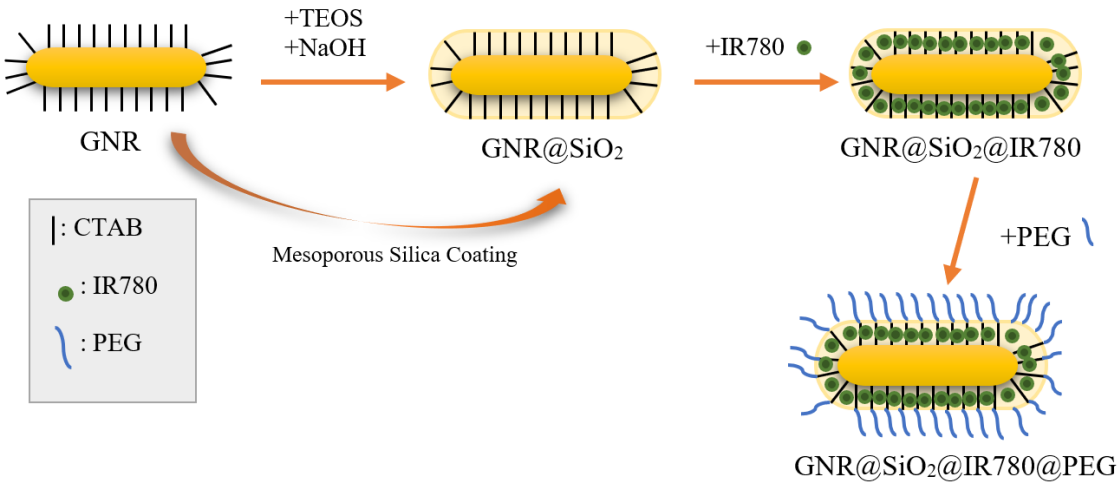


**Figure 3.4** Step-by-step synthesis of PEGylated IR780 loaded mesoporous silica coated gold nanorods ($GNRs@SiO_2@IR780@PEG$).

The optical spectrum of IR780, GNRs, $GNRs@SiO_2$, $GNRs@SiO_2@IR780$, and $GNRs@SiO_2@IR780@PEG$ was measured by using UV-VIS spectrophotometer

(NanoDrop 2000c, Thermo Scientific, MA, USA). Morphological and structural observations were obtained using Scanning Transmission Electron Microscopy (STEM) and Transmission Electron Microscopy (TEM) images and Energy Dispersive Spectrometry (EDS) analysis was used to determine the elemental composition of the nanomaterials.

IR780 content of nanoparticle was measured by using optical absorbance. The calibration curve of IR780 in ethanol was obtained at the concentration range 0.33—2.22 $\mu g$/mL where IR780 is known to follow Lambert—Beer′s Law [77]. The measurement was done at 500 nm baseline correction and the absorbance values at 780 nm were used to draw a calibration curve as seen in Figure 3.5.

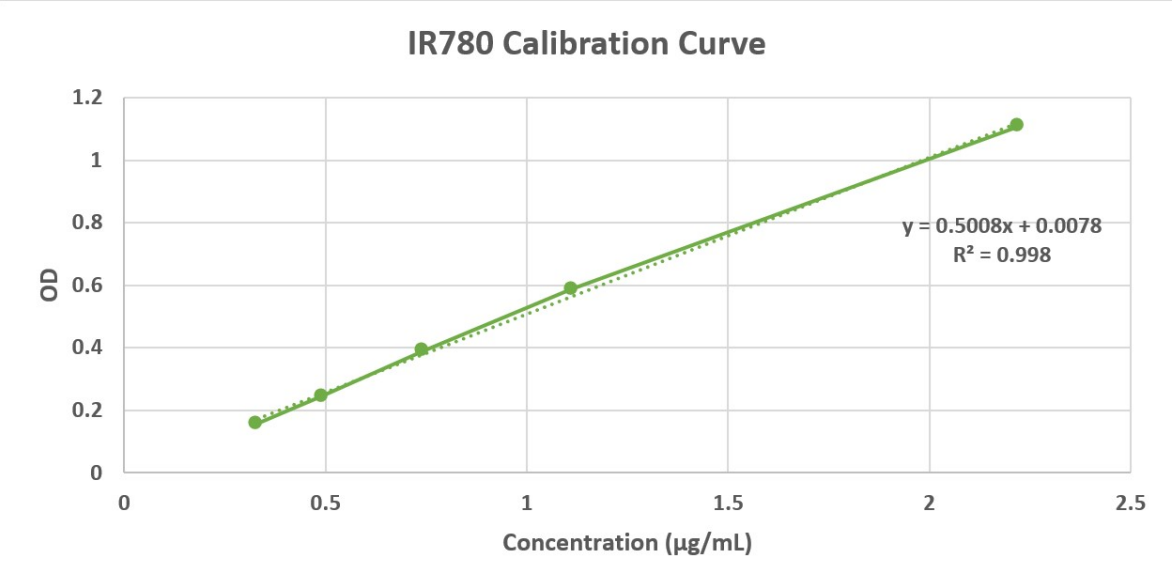


**Figure 3.5** IR780 in ethanol absorbance was recorded at 780 nm by using a spectrophotometry cuvette with a pathlength of 10 mm for the calibration curve. n=3 for each data point.

The obtained equation (Figure 3.5 (inset graphs)) from the calibration curve was used to calculate the amount of loaded and encapsulation efficiency of IR780 on the nanostructure. The calculation for the loaded amount consists of 3 parts: supernatant calculation, prepared solution calculation, and amount of the drugs. The concentration of supernatant calculation can be done by using Eq. 3.1. and Eq 3.2.

$$y(absorbance) = 0,5008 \times X_C + 0,0078 \tag{3.1}$$

This 'concentration' was found by using supernatant absorption and it is crucial to determine the concentration of the used supernatant for the measurement. To see this concentration, Eq. 3.2 was used ($C_S$: supernatant concentration, V1: taken volume of IR780 supernatant, V2: taken ethanol volume to dilute it, $X_C$: Concentration found by using Eq. 3.1).

$$C_S \times V1 = X_C \times V2 \tag{3.2}$$

After that, we need to know the concentration of the prepared solution to understand the loaded amount of the drug. The concentration of prepared solution calculation can be done by using Eq 3.3 (C1: IR780 stock concentration (mg/mL), V1: taken IR780 volume for synthesis, C2: prepared solution concentration, V2: total synthesis volume)

$$C1 \times V1 = C2 \times V2 \tag{3.3}$$

Lastly, to calculate the amount of loaded IR780, Eq. 3.4 was used and encapsulation efficiency can be calculated according to results by using Eq. 3.5, where $W_t$ is the total amount of drug in silica-coated gold nanorods and $W_i$ is the total amount of initial IR780 ($C_P$: prepared solution concentration, $C_S$: supernatant concentration).

$$\text{Amount of loaded IR780 } = C_P - C_S \tag{3.4}$$

$$\text{Encapsulation efficiency (EE \%)} = (W_t/W_i) \times 100\% \tag{3.5}$$

## 3.7 Cell Culture

In this study, the HCT116 cell line, as shown in Figure 3.6, was used as an *in vitro* colon cancer model. The HCT116 cells were cultured in T-25 cell culture flasks in Dulbecco's Modified Eagle Medium (DMEM) supplemented with 10% Fetal Bovine Serum (FBS) and 1% Penicillin-Streptomycin. They were incubated in a humidified atmosphere with 5% $CO_2$ at $37^oC$.

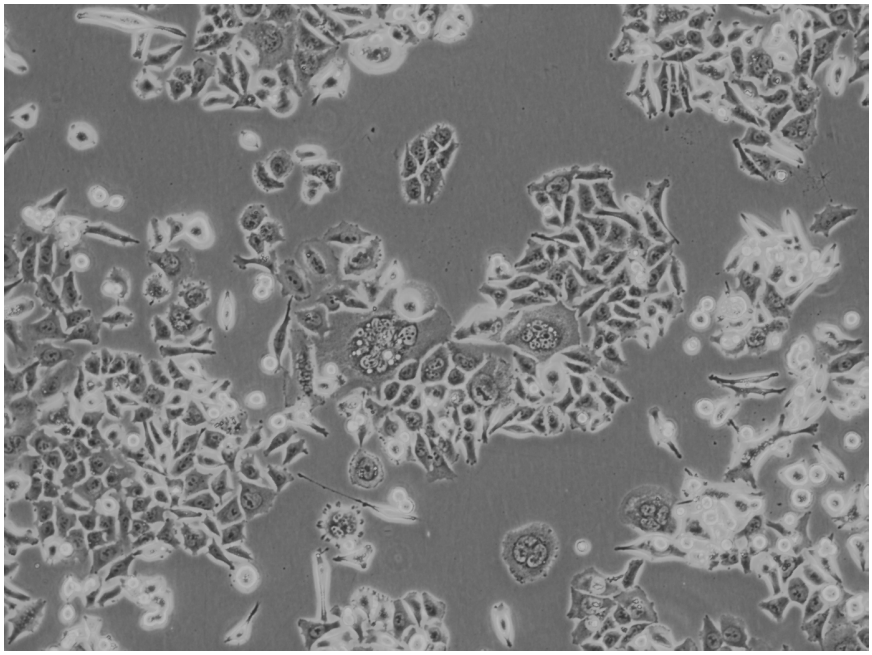

**Figure 3.6** HCT116 colon cancer cell line is imaged ZEISS Axio Vert. A1 model inverted microscope.

### 3.7.1 Cell Plating

The cells with 80-90% of confluence were detached with 0.25% trypsin EDTA solution and after harvesting, 10 $\mu$L of the suspension culture was added to the top and bottom sides of the hemocytometer to count the cells. Cells in the hemocytometer cavities were counted under an optical microscope. Based on the result and desired density ($3x10^4$ cell/well), the cell suspension was diluted, and cells were plated in 96-well plates for the control group and treatment group as shown in Figure 3.7 and Figure 3.8. For the laser-only and PDT experiments, four wells furthest from the control group were used because the most powerful area of the laser irradiation affects these wells. After cell plating, the incubator was set at $37^oC$ with 5% $CO_2$ for 24 hours for each well plate.

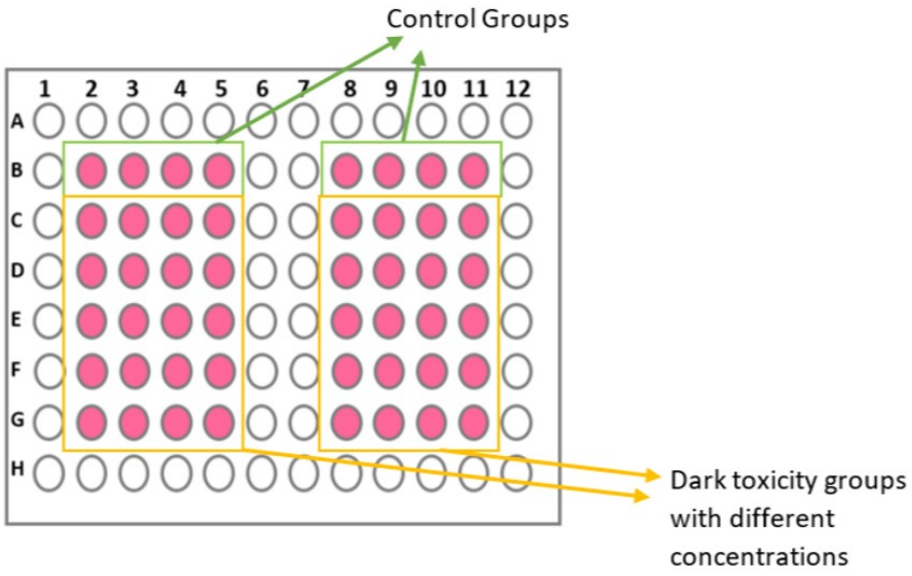


**Figure 3.7** Experiments of *in vitro* dark toxicity are shown schematically.

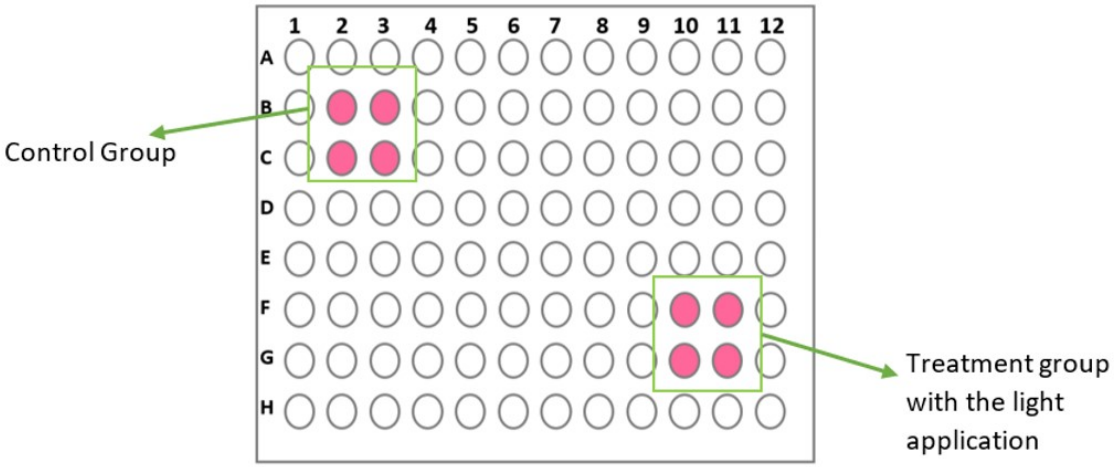


**Figure 3.8** Experiments of *in vitro* laser only and PDT are shown schematically.

## 3.8 Laser Device Set-Up

In this study, the source of light was a 785 nm diode laser system as shown in Figure 3.9 (MDL-III-785; Changchun New Industries Optoelectronics Tech. Ltd.) in continuous wave mode. Since IR780's absorption peak is at 780 nm, this diode laser was used. Before every experiment, the power density was controlled and set to 400 $mW/cm^2$.

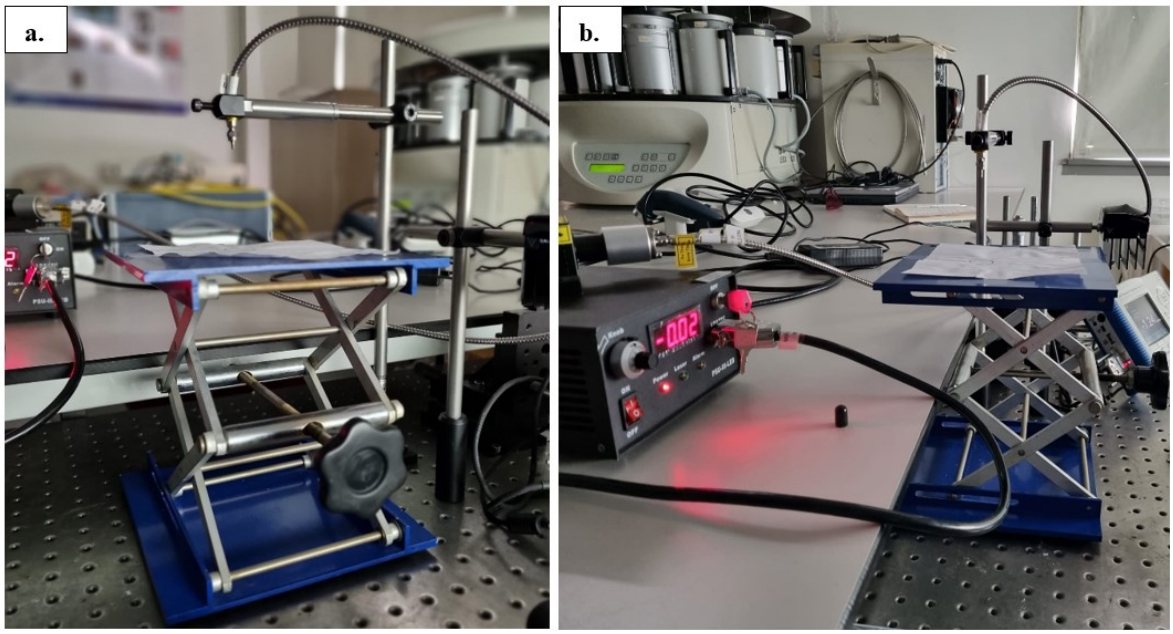


**Figure 3.9** (a, b) 785-nm diode laser system. Its components; a laser device, fiber optic cable, and adjustable board.

To find the optimum energy dose, two different power densities, 200 $mW/cm^2$ and 400 $mW/cm^2$, were examined with different application times (2.5-min, 5-min, 10-min, 20-min, and 1.25-min, 2.5-min, 5-min, 10-min, respectively). The laser energy doses were determined by using Eq. 3.6.

$$\text{Power Density} = \frac{\text{Energy Density}}{Time} \tag{3.6}$$

Thus, the energy densities were determined as 30 $J/cm^2$, 60 $J/cm^2$, 120 $J/cm^2$, and 240 $J/cm^2$. Only laser light was applied with determined four different energy doses to the cells.

## 3.9 Applications

### 3.9.1 Laser Only Groups

The medium was discarded and replaced with the new complete medium after the cells were incubated for 24 hours. Following that, cells were exposed to four energy doses of light (30 $J/cm^2$, 60 $J/cm^2$, 120 $J/cm^2$, and 240 $J/cm^2$). Control groups were shaded to prevent laser light exposure by using a black cover. After 785 nm laser exposure, the plates were placed again into the incubator for 24 hours. Then, MTT analysis was done to assess cell viability.

### 3.9.2 Dark Toxicity of $GNRs@SiO_2@IR780$

Following the 24-hour incubation period, the old media was changed with $GNRs@SiO_2@IR780$ solutions at different concentrations; 2.5 $\mu g/mL$, 5 $\mu g/mL$, 10 $\mu g/mL$, 15 $\mu g/mL$, and 25 $\mu g/mL$.

After 2 hours of incubation, the medium was removed, and Phosphate-buffered saline (PBS) was used to wash each well three times. After washing, the new complete medium was added, and the plates were placed in an incubator for 24 hours. Then, MTT analysis was done to assess cell viability.

### 3.9.3 Dark Toxicity of $GNRs@SiO_2@IR780@PEG$

Following the 24-hour incubation period, the old media was changed with $GNRs@SiO_2@IR780@PEG$ solutions at different concentrations; 2.5 $\mu g/mL$, 5 $\mu g/mL$, 10 $\mu g/mL$, 15 $\mu g/mL$, 25 $\mu g/mL$, 50 $\mu g/mL$, 100 $\mu g/mL$, 200 $\mu g/mL$, 400 $\mu g/mL$, and 500 $\mu g/mL$. Due to the PEG ligand providing much more biocompatibility, we expected the toxicity of nanoparticles to be less. Thus, the higher concentrations of nanoparticles were examined for dark toxicity.

After 2 hours of incubation, the medium was discarded, and each well was washed with PBS three times. After washing, the new complete medium was added, and the plates were placed in an incubator for 24 hours. Then, MTT analysis was done to assess cell viability.

### 3.9.4 Dark Toxicity of $GNRs@SiO_2$

Following the 24-hour incubation period, the old media was changed with $GNRs@SiO_2$ solutions at 2.5 $\mu g/mL$ concentration to compare with the dark toxicity of $GNRs@SiO_2@IR780$.

After 2 hours of incubation, the medium was discarded, and each well was washed with PBS three times. After washing, the new complete medium was added, and the plates were placed in an incubator for 24 hours. Then, MTT analysis was done to assess cell viability.

### 3.9.5 Dark Toxicity of $GNRs@SiO_2@PEG$

Following the 24-hour incubation period, the old media was changed with $GNRs@SiO_2@PEG$ solutions at 10 $\mu g/mL$ concentration to compare with the dark toxicity of $GNRs@SiO_2@IR780@PEG$.

After 2 hours of incubation, the medium was discarded, and each well was washed with PBS three times. After washing, the new complete medium was added, and the plates were placed in an incubator for 24 hours. Then, MTT analysis was done to assess cell viability.

### 3.9.6 PDT Activity of $GNRs@SiO_2@IR780$

Following the 24-hour incubation period, the old media was changed with $GNRs@SiO_2@IR780$ solutions at 2.5 $\mu g/mL$ concentration.

After 2 hours of incubation, the medium was discarded, and each well was washed with PBS three times. After washing, the new complete medium was added, and PDT treatment groups were illuminated with 785 nm laser light at 400 $mW/cm^2$ for 10 min on the setup. Control groups were shaded to prevent laser light exposure by using a black cover. After the PDT experiment, the 96-well plates were placed in an incubator for 24 hours. Then, MTT analysis was done to assess cell viability.

### 3.9.7 PDT Activity of $GNRs@SiO_2@IR780@PEG$

Following the 24-hour incubation period, the old media was changed with $GNRs@SiO_2@IR780@PEG$ solutions at concentration 10 $\mu g/mL$.

After 2 hours of incubation, the medium was discarded, and each well was washed with PBS three times. After washing, the new complete medium was added, and PDT treatment groups were illuminated with 785 nm laser light at 400 $mW/cm^2$ for 10 min on the setup. Control groups were shaded to prevent laser light exposure by using a black cover. After the PDT experiment, the 96-well plates were placed in an incubator for 24 hours. Then, MTT analysis was done to assess cell viability.

### 3.9.8 PDT Activity of $GNRs@SiO_2$

Following the 24-hour incubation period, the old media was changed with $GNRs@SiO_2$ solutions at concentration 2.5 $\mu g/mL$ to compare with the PDT activity of $GNRs@SiO_2@IR780$.

After 2 hours of incubation, the medium was discarded, and each well was washed with PBS three times. After washing, the new complete medium was added, and PDT treatment groups were illuminated with 785 nm laser light at 400 $mW/cm^2$ for 10 min on the setup. Control groups were shaded to prevent laser light exposure by using a black cover. After the PDT experiment, the 96-well plates were placed in an incubator for 24 hours. Then, MTT analysis was done to assess cell viability.

### 3.9.9 PDT Activity of $GNRs@SiO_2@PEG$

Following the 24-hour incubation period, the old media was changed with $GNRs@SiO_2@PEG$ solutions at concentration 10 $\mu g/mL$ to compare with the PDT activity of $GNRs@SiO_2@IR780@PEG$.

After 2 hours of incubation, the medium was discarded, and each well was washed with PBS three times. After washing, the new complete medium was added, and PDT treatment groups were illuminated with 785 nm laser light at 400 $mW/cm^2$ for 10 min on the setup. Control groups were shaded to prevent laser light exposure by using a black cover. After the PDT experiment, the 96-well plates were placed in an incubator for 24 hours. Then, MTT analysis was done to assess cell viability.

## 3.10 MTT Analysis

After all experimental approaches, the cells will be incubated for 24 hours. 10 $\mu L$ MTT solution will be added to each well for the assessment of cell viability. After 3 hours of incubation, the media will be removed after 3 hours of incubation, and each well will receive 100 $\mu L$ DMSO. Then, the plate will be put on the shaker for 15 minutes and placed in the optical reader device. By measuring the difference between the absorption at 570 nm and 760 nm wavelengths on the micro-plate reader, the OD was found, and results were compared with a control group that was not irradiated with light or incubated with a photosensitizer.

## 3.11 Statistical Analysis

The IBM SPSS Statistics program was used for the statistical analysis to find the significant differences between each group. First, to verify whether all the measured data is normally distributed or not, the Shapiro-Wilk test was implemented. One-Way ANOVA (Analysis of Variance) is a feasible option if the dependent variable has a normal distribution. Since our all data is normally distributed in this study, One-Way ANOVA with the Bonferroni post hoc test was performed for identifying the significantly different groups. All tests were considered as *$p<0.05$ to be statistically significant.

# 4. RESULTS

In this section, we will report the obtained results from the *in vitro* experiments and characterization experiments. The parameters of the experiments were set in a one-factor-at-a-time plan to optimize the experimental design.

## 4.1 Characterization of Nanoparticles

### 4.1.1 UV-Vis Spectroscopy (UV-Vis)

UV-Vis Spectroscopy, also known as Spectrophotometry, is a quantitative technique to measure the light absorption in a solution. This measurement is done by comparing the quantity of light that passes through a sample to the amount of light that passes through a reference sample or a blank as shown in Figure 4.1.

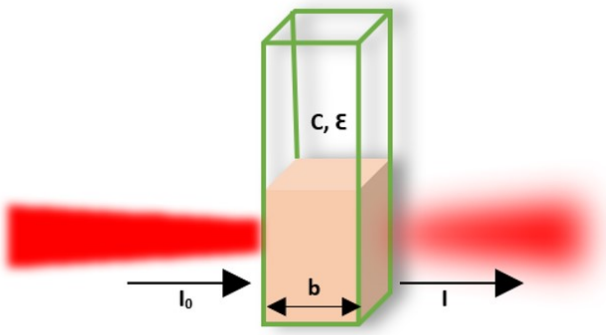


**Figure 4.1** The response of a sample, when exposed to electromagnetic radiation in the ultraviolet and visible range, is measured by UV-visible spectroscopy. The Beer-Lambert law, which is illustrated in Eq. 4.1, could be used to characterize the intensities of receiving light ($I_0$) and transmitting light ($I$). The molar absorptivity is represented by the symbol $\in$ ($Lmol^{-1}cm^{-1}$); the pathlength in cm is represented by the symbol b, and the concentration in mol/L is represented by the symbol c.

$$A = -logT = -log\frac{I}{I_0} = \in bc \tag{4.1}$$

In seed-mediated of GNRs, the cationic surfactant CTAB, which contains a hydrophilic cationic head group and a hydrophobic tail, has typically been utilized as a stabilizing agent to control the formation of an anisotropic shape [69]. In particular, the complex $CTA-AgBr_2^-$ (referred to as CTASB) that results from the use of $AgNO_3$ as a shape-directing agent prevents growth along the transversal axis [69, 78]. Silver nitrate is known to promote anisotropy and increase yield during the creation of gold nanorods [69]. The type of the seeds and the growth environment interact intricately, leading to the development of anisotropy. Because of this, achieving a final state with a homogenous size and shape distribution is rather challenging. Experimentally, post-synthetic purification processes are always required since isotropic structures inevitably contaminate the syntheses of anisotropic shapes. After a protracted purifying process involving high-speed centrifugation, the monodisperse GNRs are often produced [69, 79, 80].

Gold nanorods have two plasmon resonances caused by light absorption and scattering on different axis of the nanorod. A transverse surface plasmon resonance (T-SPR) occurs along the short axis of the rod, and longitudinal surface plasmon resonance (L-SPR), occurs along the long axis of the rods. The latter is highly adjustable in the NIR and visible spectrum and varies linearly on aspect ratio. UV-Vis spectra reveal two well-separated unique plasmon peaks with the features of anisotropic morphologies, T-SPR (512 nm) and L-SPR (741 nm) as shown in Figure 4.2. Additionally, after silica coating, the longitudinal SPR peak (766 nm) shows a small redshift (22 nm) as expected.

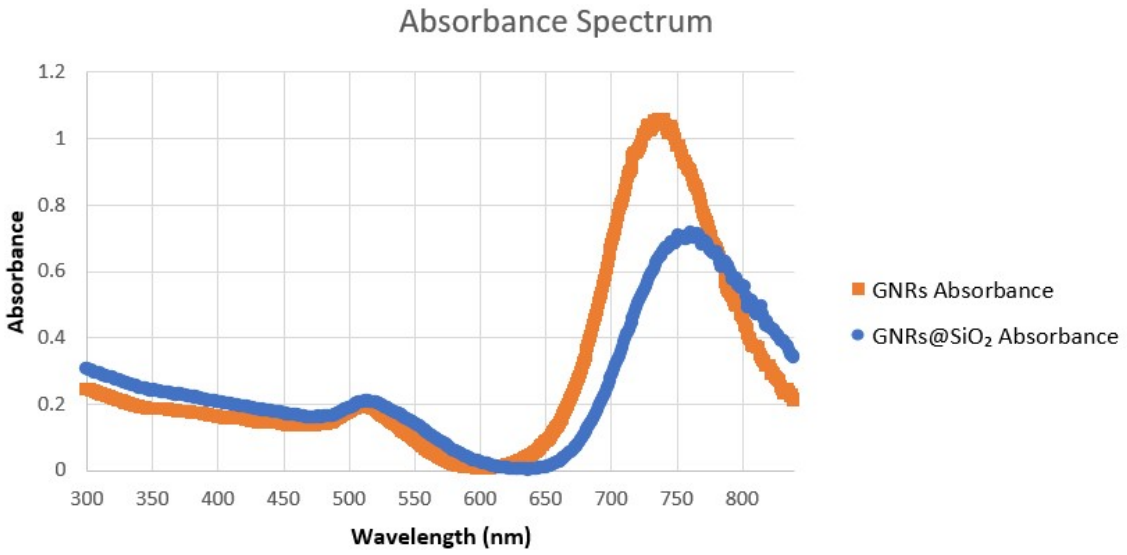


**Figure 4.2** Absorption spectrum of GNRs and $GNRs@SiO_2$ nanoparticles.

Moreover, the aspect ratio (AR), the ratio of a GNR's width to height, can be calculated by using the maximum absorption obtained from the spectrum. Eq. 4.2 represents the relation between AR and L-SPR absorption maximum ($\lambda$max) [69].

$$AR = (\frac{\lambda_{max} - 478)}{96} \tag{4.2}$$

### 4.1.2 TEM and EDS Analysis

TEM was used to observe the shape and average size of the nanoparticles. We can examine the smaller particles with higher resolution ($\sim$ 0.2 nm) than Scanning Electron Microscopy (SEM). Solutions needed to be diluted to observe high-resolution images and TEM images were taken by operating Jeol JEM-2100PLUS TEM (Figure 4.3).

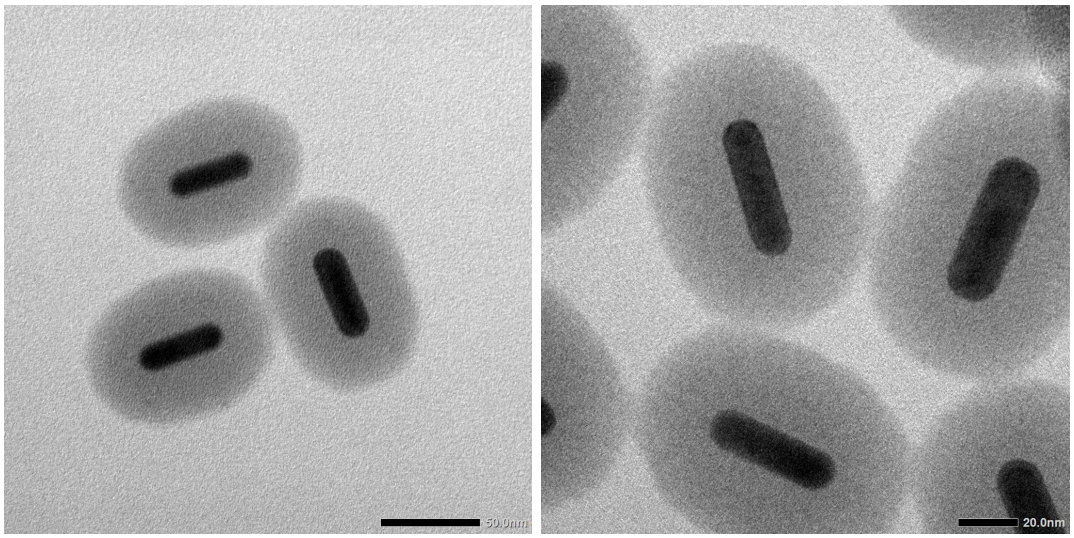


**(a)** **(b)**

**Figure 4.3** TEM images of (a, b) $GNRs@SiO_2$ in 50 nm and 20 nm, respectively.

By using these TEM images, we performed the particle size analyses by using ImageJ software. While the whole particle size is approximately 100 nm, the gold nanorod′s length is 50 nm as shown in Figure 4.4. The width of the whole particle is about 66 nm, and the silica coating is fairly evenly around the rod′s circumference.

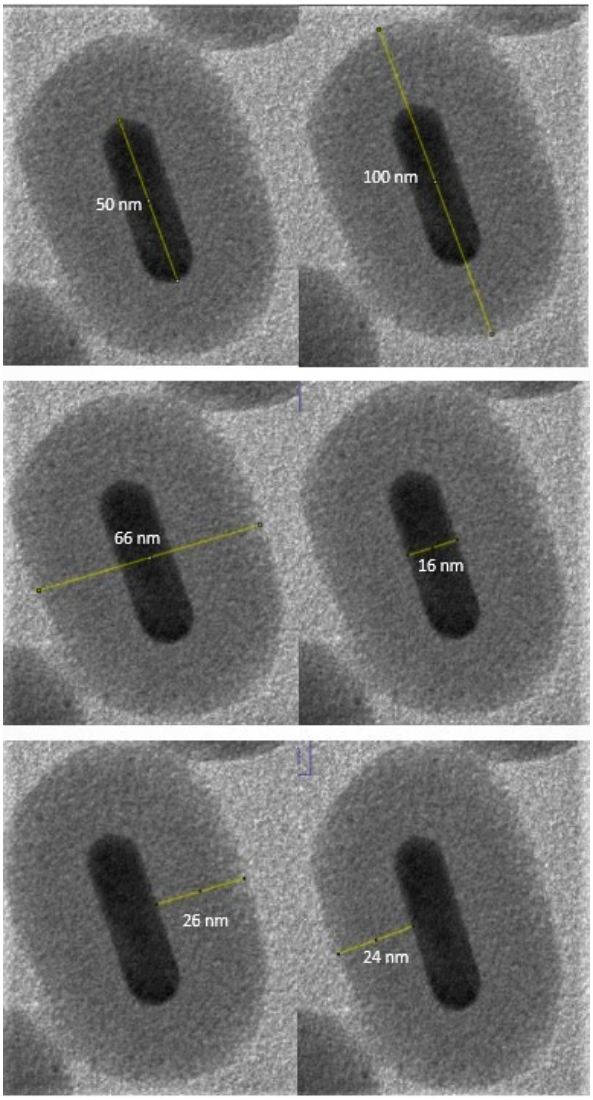


**Figure 4.4** The particle size analysis by using ImageJ software.

Additionally, EDS analysis results of elemental mapping of O, Si, and Au elements that were inside the nanostructure. EDS analysis showed that while gold electrons seem the core of the particle, silica electrons seem a coating around the gold core (Figure 4.5).

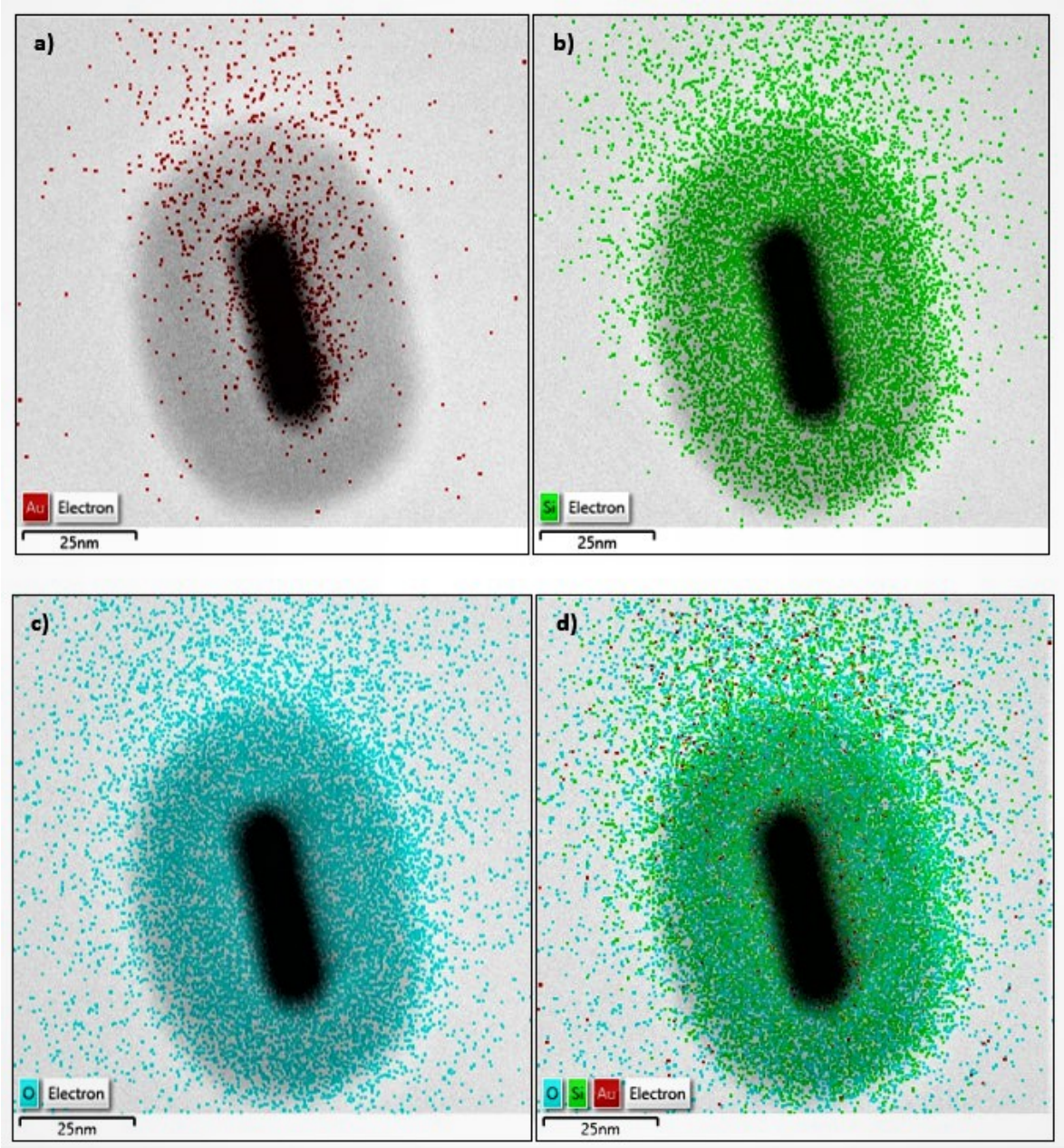


**Figure 4.5** (a) EDS electron image for elemental mapping of gold (Au) (the red dots), (b) elemental mapping of silicon (Si) (the green dots), (c) elemental mapping of oxygen (O) (the blue dots), (d) EDS mapping for Au, Si, O elements of $GNRs@SiO_2$ nanostructure.

EDS spectrum analysis also was performed, and corresponding peaks were shown in Figure 4.6 as the weight percentage of the elements on particles.

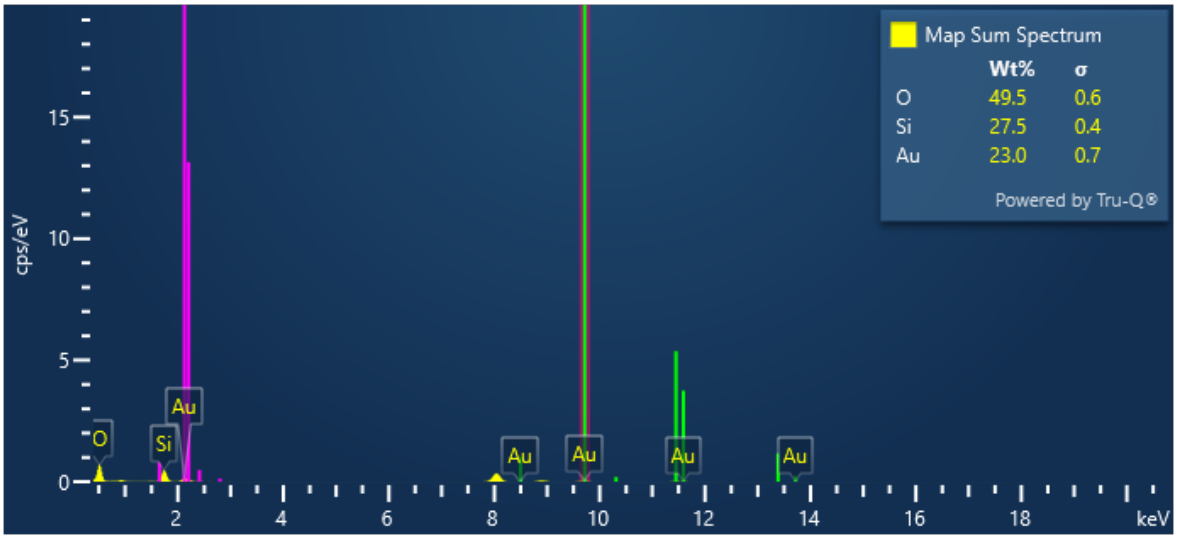


**Figure 4.6** EDS map sum spectrum analysis of scanned $GNRs@SiO_2$ particles as weight percentage for Si, Au, and O. Weight percentage (Wt%) shows the weight of an element in percent.

### 4.1.3 STEM Analysis

STEM analysis also provides to investigate silica coating on GNRs as TEM analysis. The STEM images were taken by operating FEI-Philips XL30 ESEM-FEG SEM at 10.0 kV as shown in Figure 4.7. Two types of detectors were used, Backscattered electrons (BSE) and Secondary electrons (SE) detectors. We can obtain more detailed surface information by using an SE detector.

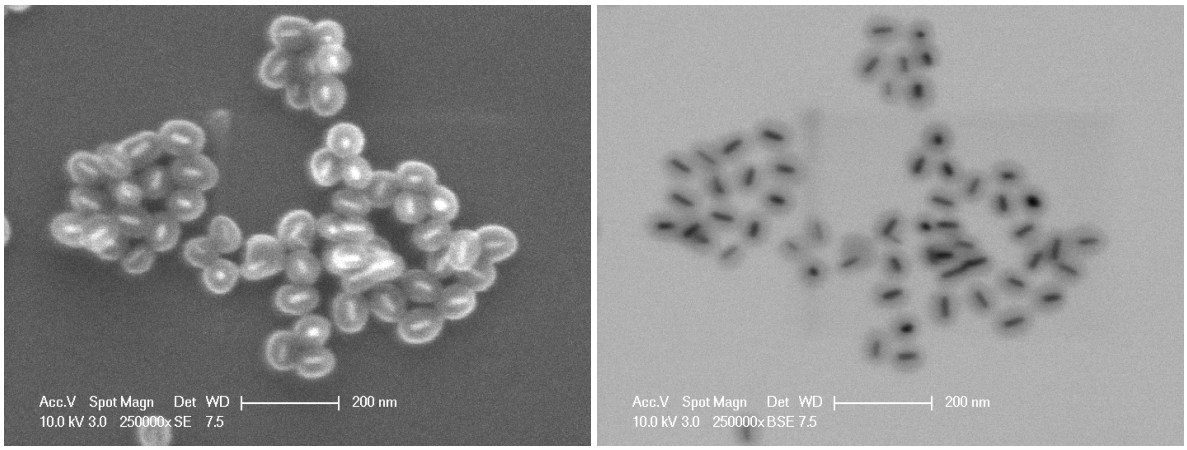


**(a)** **(b)**

**Figure 4.7** STEM images were taken by using SE detector (a) and BSE detector (b).

Additionally, the thickness of silica and length of GNRs and silica-coated GNRs were measured as shown in Figure 4.8. The silica coating thickness is about 22-23 nm, the length of GNRs is about 30-32 nm, and the length of silica-coated GNRs ranges from 77 to 91 nm. These measurements show that the nanostructures are monodisperse.

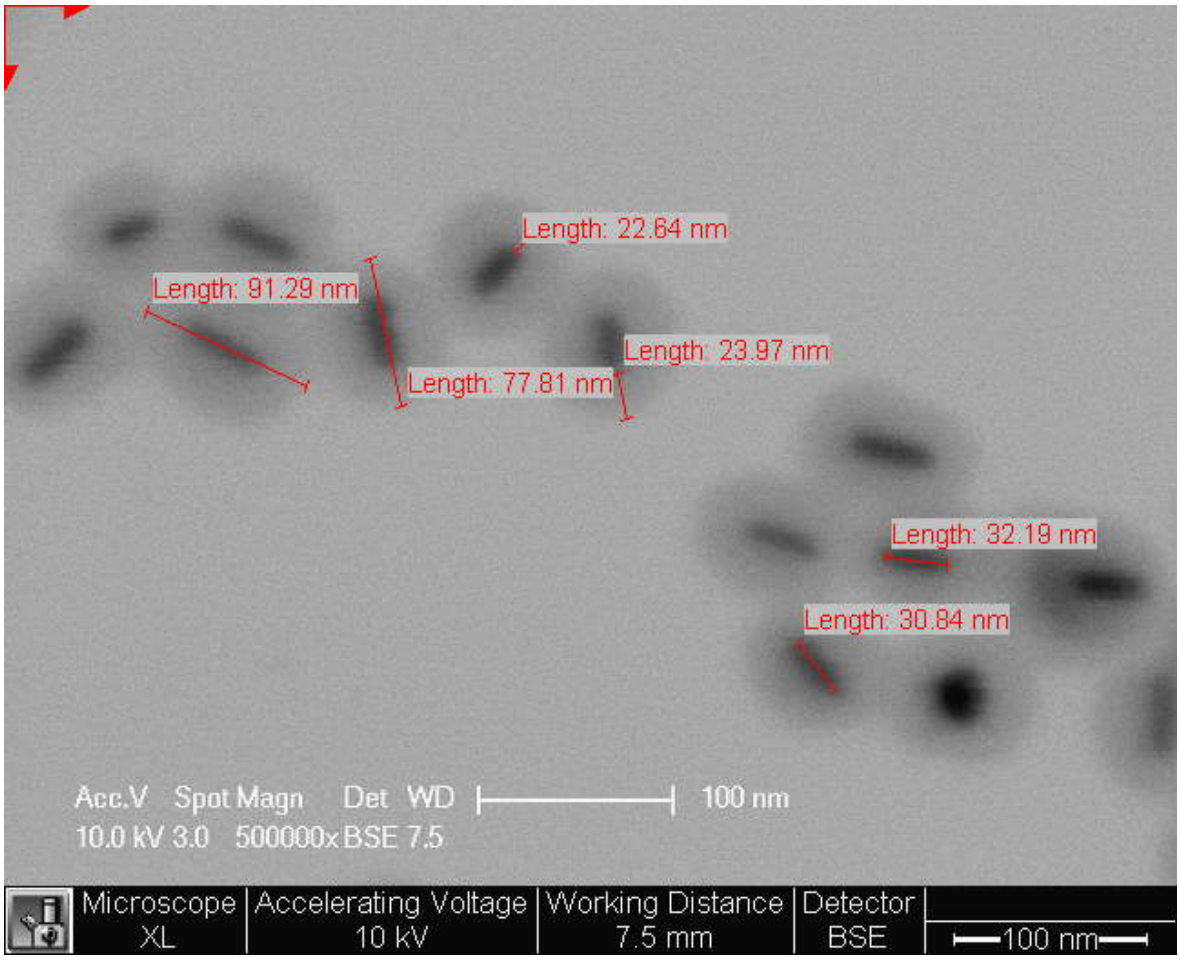


**Figure 4.8** STEM images of the length measurements of the thickness of silica and length of GNRs and silica-coated GNRs.

### 4.1.4 Fourier Transform Infrared (FTIR) Analysis

Fourier Transform Infrared (FTIR) spectra were collected by using a Bruker FTIR Spectrometer, Tensor 27 model with ATR module, with wavenumbers ranging from 400 to 4000 $cm^{-1}$ [81]. In this way, we can observe the chemical properties of synthesized nanoparticles. The FTIR spectra of GNRs show two bands at ∼2360 and ∼2350 $cm^{-1}$ (C-H bond alkanes stretch) due to the asymmetrical and symmetrical vibrations of $CH_2$ from CTAB molecules as shown in Figure 4.9. After the silica coating of GNRs, since Si-O bands have strong absorption between 830 and 1110 $cm^{-1}$, FTIR spectra show a peak at ∼1076 $cm^{-1}$ as shown in Figure 4.10. The FTIR spectra of IR780 have a peak at ∼1045 $cm^{-1}$ (Figure 4.11) and this peak can be also seen in the

FTIR spectra of $GNRs@SiO_2@IR780$ (Figure 4.12) [76, 81, 82].

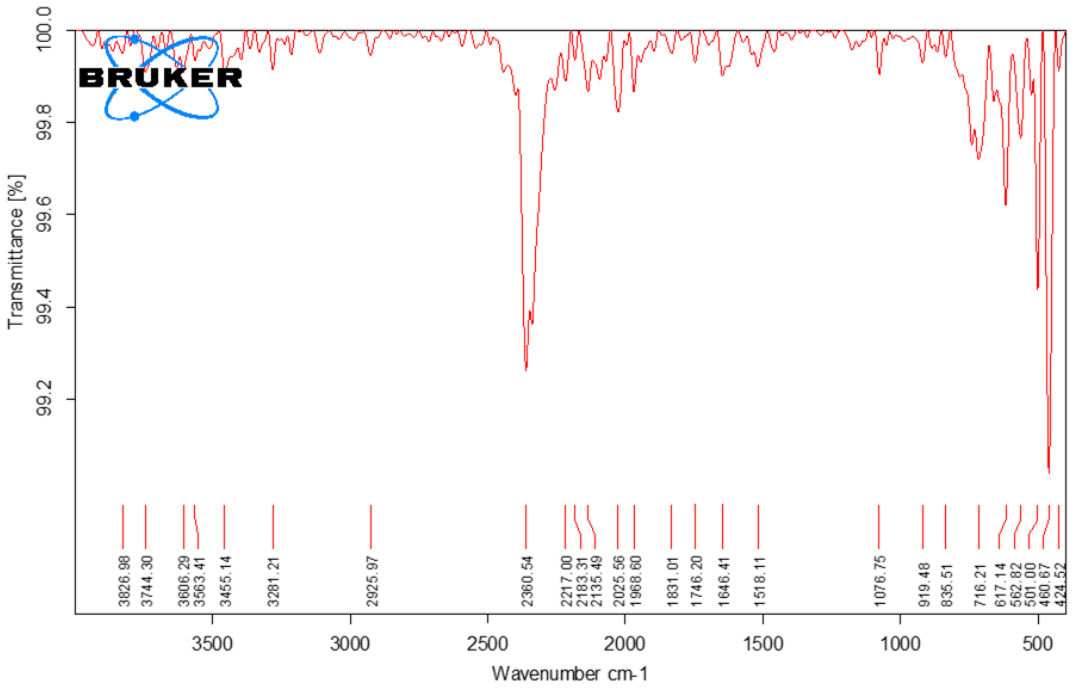


**Figure 4.9** FTIR spectra of GNRs

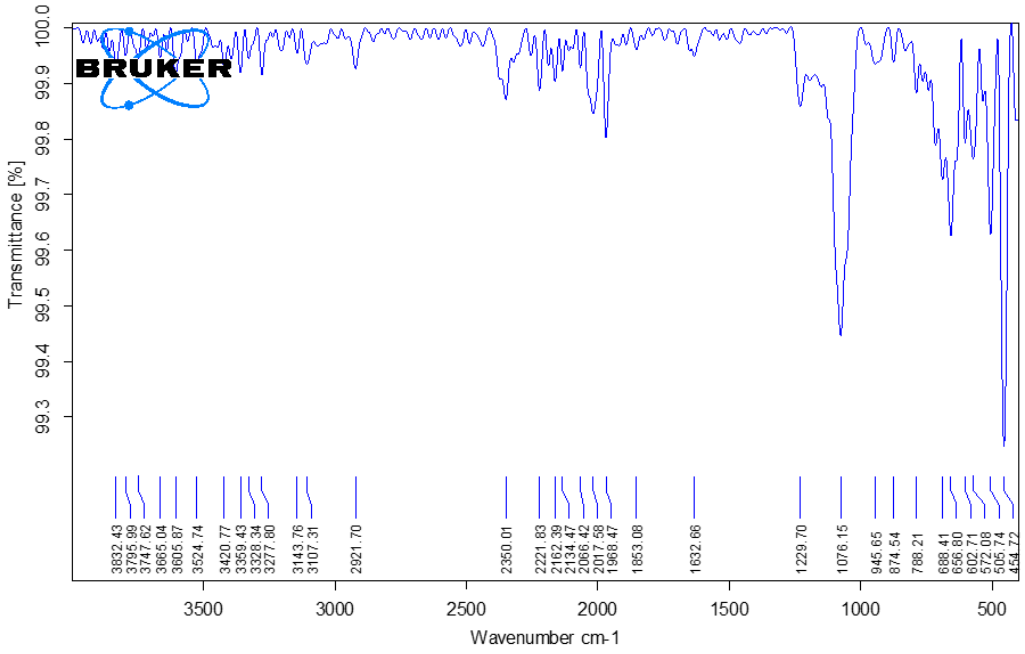


**Figure 4.10** FTIR spectra of $GNRs@SiO_2$

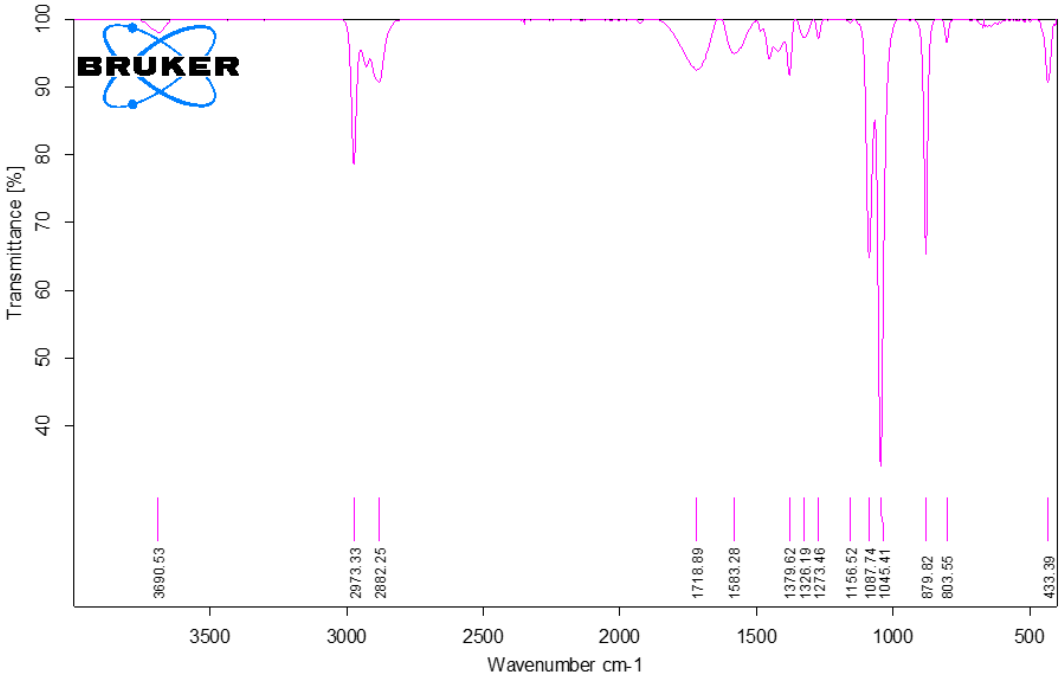


**Figure 4.11** FTIR spectra of IR780

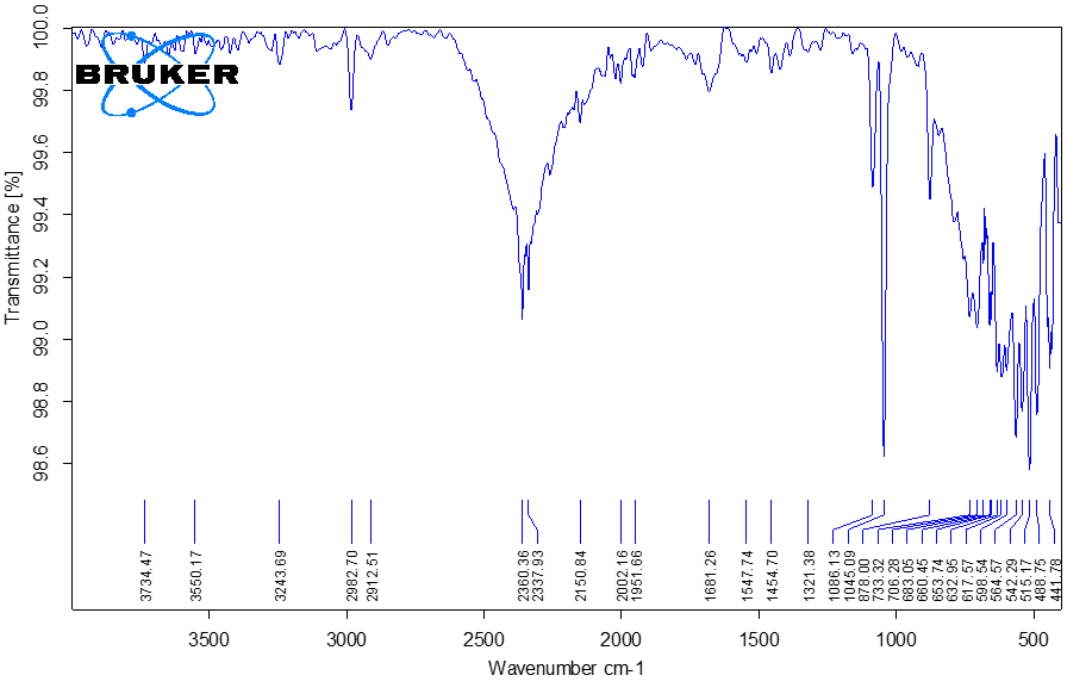


**Figure 4.12** FTIR spectra of $GNRs@SiO_2@IR780$

### 4.1.5 IR780 Loading Efficiency

The absorbance value at 780 nm is 0.328 for IR780 at 500 nm baseline correction. The equations were given in part 3.6. Firstly, the supernatant concentration is calculated:

$$0,328 = 0,5008 \times X_C + 0,0078 => X_C \quad = Concentration = 0,6393769968 \mu g/mL$$

This concentration is calculated by taking 5 $\mu$L supernatant and 1495 $\mu$L ethanol, so we need to consider the dilution rate:

$$C_S \times (5 \mu L) = X_C \times (1500 \mu L)$$
$$C_S \times (5 \mu L) = (0,6393769968 \mu g/mL) \times (1500 \mu L)$$
$$C_S = 191,81309904 \mu g/mL$$

To calculate the difference between supernatant and prepared solution, we need to know the prepared solution concentration. The synthesis was done by using 2.5 mL IR780 (1 mg/mL), and 7 mL $GNRs@SiO_2$ in ethanol:

$$C1 \times V1 = C2 \times V2$$
$$(1 mg/mL) \times (2.5 mL) = C2 \times (9.5 mL)$$

$$C2 = 0,2631578947 mg/mL \qquad = 263,1578947 \mu g/mL$$

After this calculation, the amount of drug can be calculated:

$$C_P - C_S = 263,1578947 \mu g/mL - 191,81309904 \mu g/mL \quad = 71,34479566 \mu g/ml$$

Thus, we can say that 5.3 mg $GNRs@SiO_2$ contains 71,34479566 $\mu$g IR780 and the loading efficiency can be calculated:

$$\text{Encapsulation Efficiency (EE \%)} = \frac{71,34479566}{263,1578947} \times 100 \qquad = 27,11\%$$

## 4.2 Applications

### 4.2.1 Laser Only Groups

The cells were exposed by using 785 nm laser light with the constant power of 200 $mW/cm^2$ but different durations: 2.5 min, 5 min, 10 min, and 20 min. Therefore, the energy densities can be calculated as 30 $Joule/cm^2$, 60 $Joule/cm^2$, 120 $Joule/cm^2$, and 240 $Joule/cm^2$, respectively. Following exposure to light, the cell viability did not decrease below 85% and there was no significantly different group in comparison to a control group that was not irradiated with light as shown in Figure 4.13.

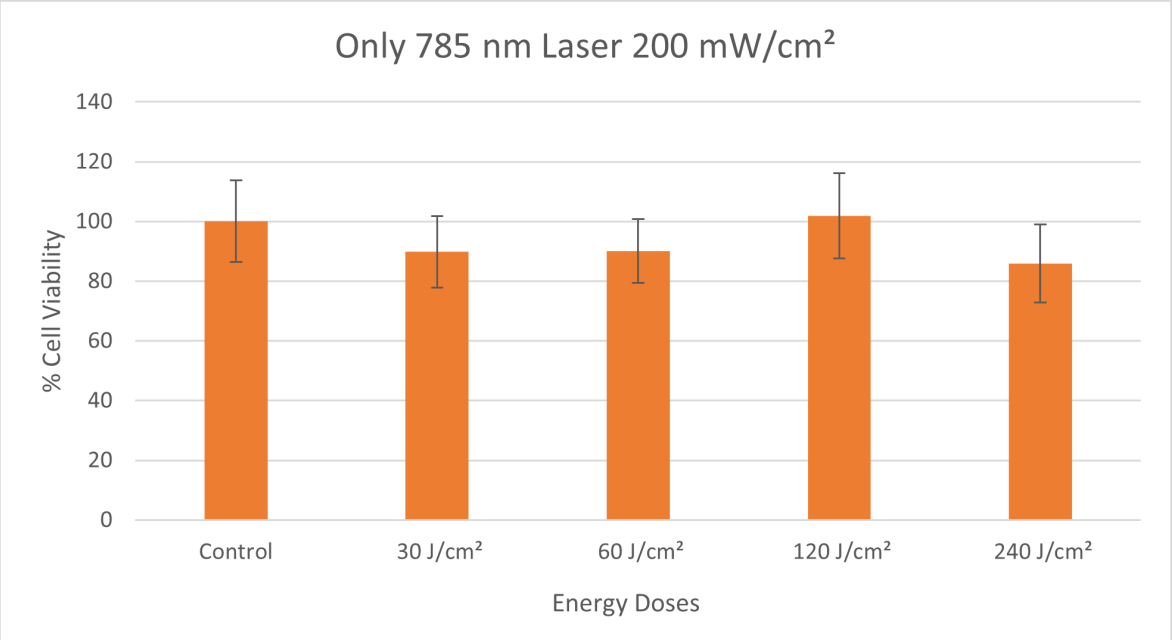


**Figure 4.13** Laser-only groups. Cells were exposed by using a red laser with a 785 nm wavelength at a power density of 200 $mW/cm^2$, and energy doses of 30 $Joule/cm^2$ (2.5 min), 60 $Joule/cm^2$ (5 min), 120 $Joule/cm^2$ (10 min), and 240 $Joule/cm^2$ (20 min).

Another laser-only group experiment was done by using 785 nm laser light at a power density of 400 $mW/cm^2$. The cells were exposed by using 785 nm laser light with the constant power of 400 $mW/cm^2$ but different durations: 1.25 min, 2.5 min, 5 min, and 10 min. However, the energy densities can be calculated the same as the experiment of only laser at 200 $mW/cm^2$: 30 $Joule/cm^2$, 60 $Joule/cm^2$, 120 $Joule/cm^2$, and 240 $Joule/cm^2$, respectively. Following exposure to light, the cell viability did not decrease below 95% and there was no significantly different group compared with a control group which was not irradiated with light as shown in Figure 4.14. After this experiment, the power density of 400 $mW/cm^2$ and 10 minutes duration were chosen to analyze them in PDT applications.

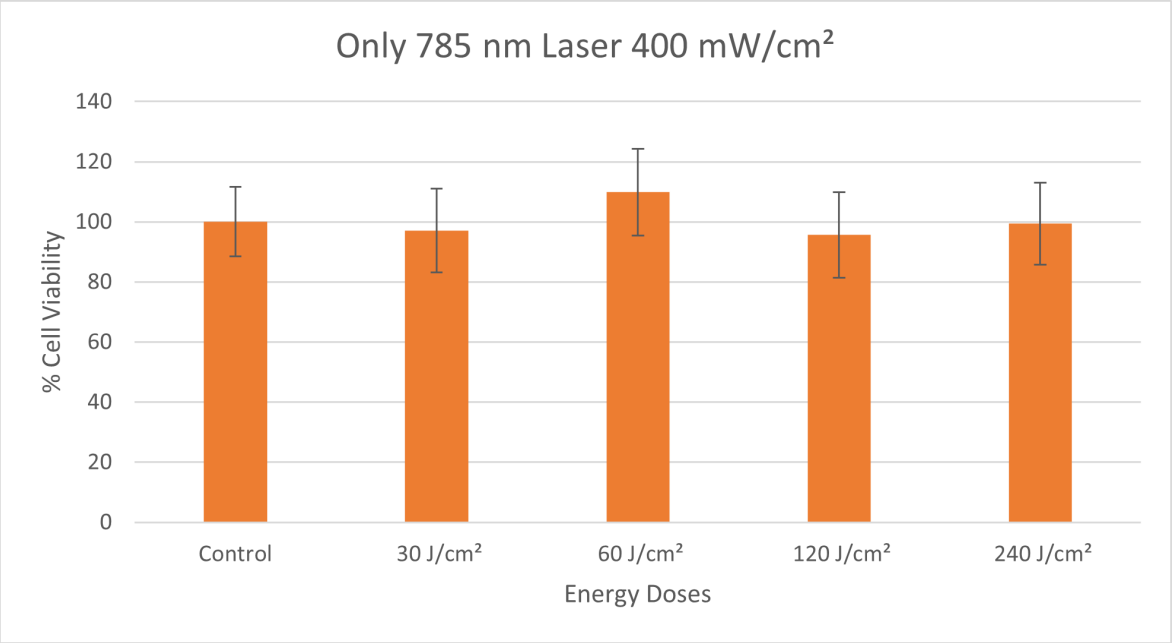


**Figure 4.14** Laser-only groups. Cells were exposed by using a red laser with a 785 nm wavelength at a power density of 400 $mW/cm^2$, and energy doses of 30 $Joule/cm^2$ (1.25 min), 60 $Joule/cm^2$ (2.5 min), 120 $Joule/cm^2$ (5 min), and 240 $Joule/cm^2$ (10 min).

### 4.2.2 Dark Toxicity of $GNRs@SiO_2@IR780$

The cells were treated with only $GNRs@SiO_2@IR780$ at different concentrations, 2.5 $\mu$g/mL, 5 $\mu$g/mL, 10 $\mu$g/mL, 15 $\mu$g/mL, and 25 $\mu$g/mL for 2 hours. When data are compared with a control group that had no treatment, the cell viability was below 80% after the concentration of 5 $\mu$g/mL of $GNRs@SiO_2@IR780$ as shown in Figure 4.15. It can be said that only $GNRs@SiO_2@IR780$ does not show any dark toxicity effect on cancer cells at 2.5 $\mu$g/mL and 5 $\mu$g/mL. However, 5 $\mu$g/mL of $GNRs@SiO_2@IR780$ showed a significantly different as compared with a control group. After this experiment, the $GNRs@SiO_2@IR780$ concentration of 2.5 $\mu$g/mL was chosen to analyze it in the PDT application.

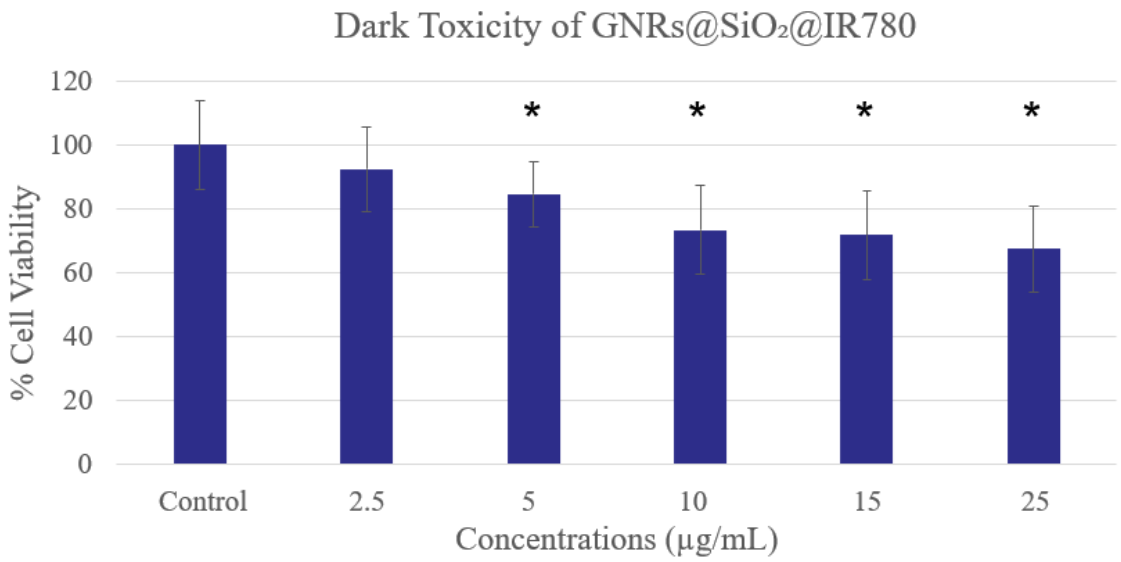


**Figure 4.15** Only $GNRs@SiO_2@IR780$ groups. The cells were incubated for 2 hours with different concentrations of $GNRs@SiO_2@IR780$, 2.5 $\mu$g/mL, 5 $\mu$g/mL, 10 $\mu$g/mL, 15 $\mu$g/mL, and 25 $\mu$g/mL. * Shows that the group is statistically significant ($p < 0.05$) compared to the control group which received no incubation with $GNRs@SiO_2@IR780$.

### 4.2.3 PDT Activity of $GNRs@SiO_2@IR780$

Firstly, the cells were treated with $GNRs@SiO_2@IR780$ at a concentration of 2.5 $\mu$g/mL for 2 hours. After incubation, and washing the cells, the fresh media was added, and a 785 nm laser was used to irradiate cells for 10 minutes at 400 $mW/cm^2$. When data are compared with the control group which received no treatment, the cell viability was 59% as shown in Figure 4.16. It can be said that we could decrease the HCT116 colon cancer cell viability by about 40% by applying PDT with $GNRs@SiO_2@IR780$ at 2.5 $\mu$g/mL.

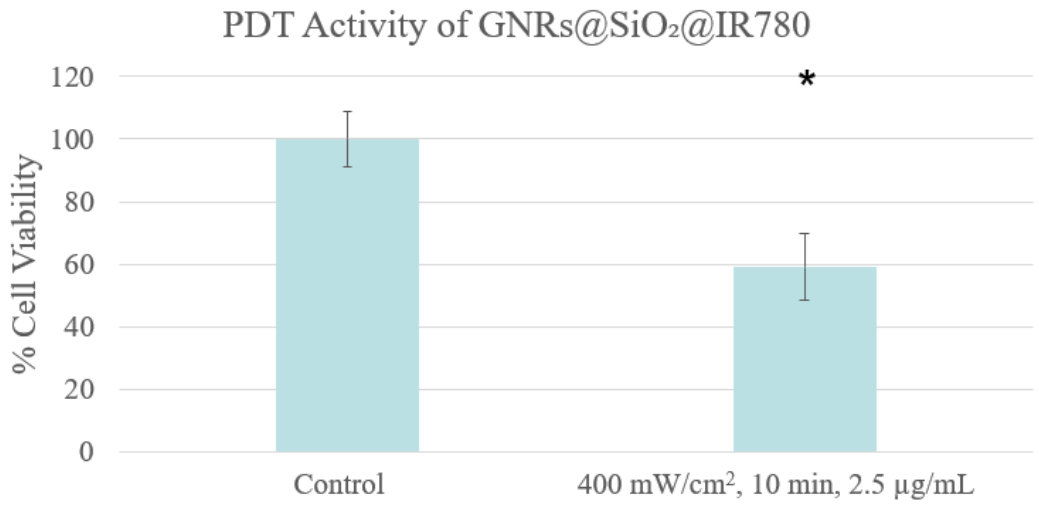


**Figure 4.16** The PDT activity to HCT116 cells by exposing a 785 nm laser light for 10 min at a power density of 400 $mW/cm^2$ and the concentration of $GNRs@SiO_2@IR780$ is 2.5 $\mu$g/mL. We cannot perform the post hoc test in this experiment because we have fewer than three groups. That's why the independent Independent-Samples T-Test analysis was performed. * Shows that the group is statistically significant ($p < 0.05$) compared to the control group which received no incubation with $GNRs@SiO_2@IR780$.

### 4.2.4 Dark Toxicity of $GNRs@SiO_2$ and PDT Activity of $GNRs@SiO_2$

The cells were treated with only $GNRs@SiO_2$ for a dark toxicity experiment at a concentration of 2.5 $\mu$g/mL for 2 hours to see the IR780 effect of PDT application of $GNRs@SiO_2@IR780$. When data are compared with a control group that had no treatment, the cell viability was 79.34% as shown in Figure 4.17. It can be said that only $GNRs@SiO_2$ does not show any dark toxicity effect on cancer cells at 2.5 $\mu$g/mL. After this experiment, the PDT activity of $GNRs@SiO_2$ was done by incubating the cells with $GNRs@SiO_2$ at a concentration of 2.5 $\mu$g/mL for 2 hours. After incubation, and washing the cells, the fresh media was added, and a 785 nm laser was used to expose cells for 10 minutes at 400 $mW/cm^2$. When data are compared with a control group that received no treatment, the cell viability was 86.47% as shown in Figure 4.18.

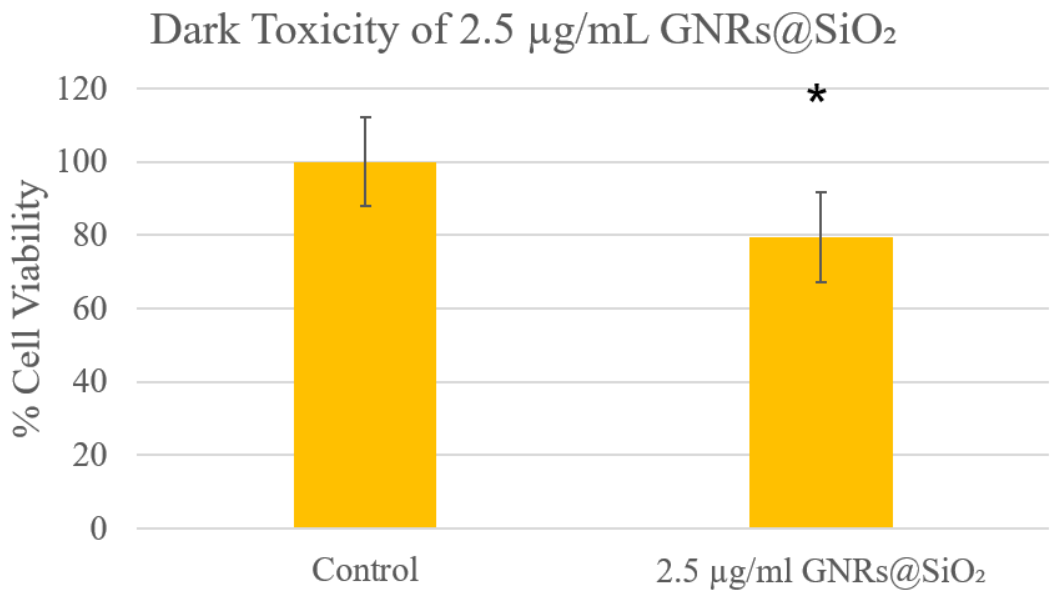


**Figure 4.17** The dark toxicity experiment of 2.5 $\mu$g/mL $GNRs@SiO_2$. We cannot perform the post hoc test in this experiment because we have fewer than three groups. That's why the independent Independent-Samples T-Test analysis was performed. * Shows that the group is statistically significant ($p < 0.05$) compared to the control group which received no incubation with $GNRs@SiO_2$.

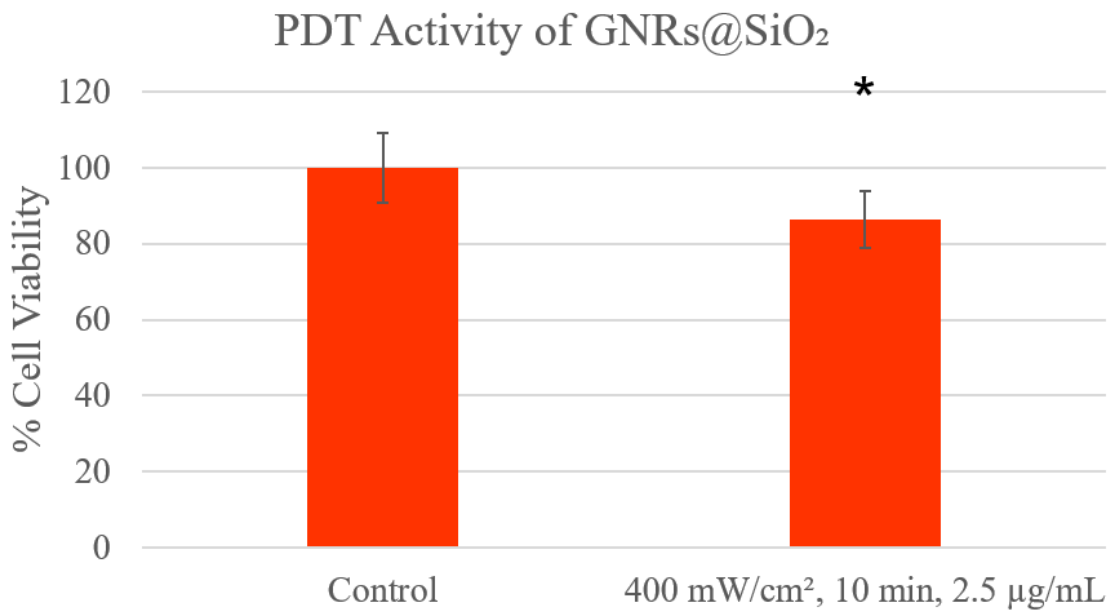


**Figure 4.18** The PDT activity to HCT116 cells by exposing a 785 nm laser light for 10 min at a power density of 400 $mW/cm^2$ and the concentration of $GNRs@SiO_2$ is 2.5 $\mu$g/mL. We cannot perform the post hoc test in this experiment because we have fewer than three groups. That's why the independent Independent-Samples T-Test analysis was performed. * Shows that the group is statistically significant ($p < 0.05$) compared to the control group which received no incubation with $GNRs@SiO_2$.

### 4.2.5 Dark Toxicity of $GNRs@SiO_2@IR780@PEG$

The cells were treated with only $GNRs@SiO_2@IR780@PEG$ at different concentrations, 2.5 $\mu$g/mL, 5 $\mu$g/mL, 10 $\mu$g/mL, 15 $\mu$g/mL, 25 $\mu$g/mL, 50 $\mu$g/mL, 100 $\mu$g/mL, 200 $\mu$g/mL, 400 $\mu$g/mL, and 500 $\mu$g/mL for 2 hours. When data are compared with a control group that had no treatment, the cell viability was less than 80% following the 25 $\mu$g/mL concentration of $GNRs@SiO_2@IR780@PEG$ as shown in Figure 4.19. It can be said that only $GNRs@SiO_2@IR780@PEG$ does not show any dark toxicity effect on cancer cells at 2.5 $\mu$g/mL, 5 $\mu$g/mL, 10 $\mu$g/mL, and 15 $\mu$g/mL. However, 15 $\mu$g/mL of $GNRs@SiO_2@IR780@PEG$ showed a significantly different as compared with a control group. After this experiment, the $GNRs@SiO_2@IR780@PEG$ concentration used for the PDT activity experiment was 10 $\mu$g/mL.

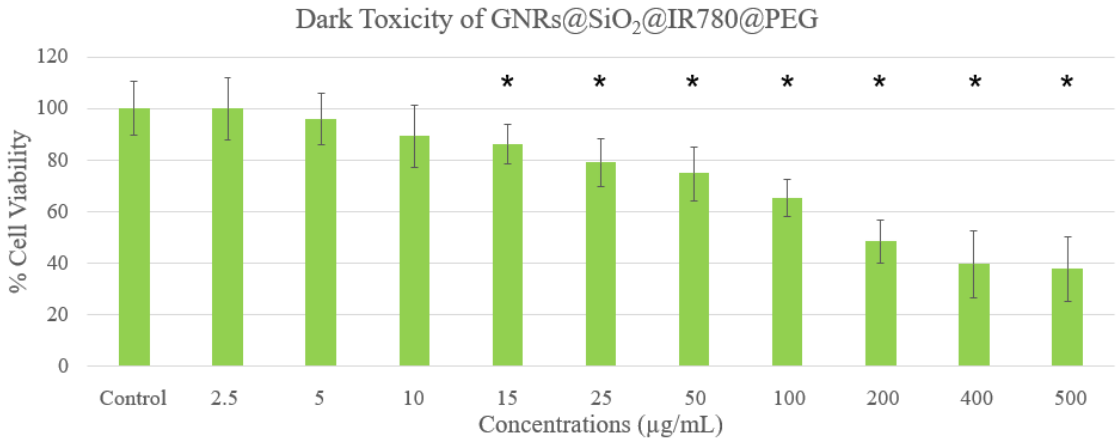


**Figure 4.19** Only $GNRs@SiO_2@IR780@PEG$ groups. Cells were incubated with $GNRs@SiO_2@IR780@PEG$ for 2 hours at different concentrations from 2.5 $\mu$g/mL to 500 $\mu$g/mL. *Shows that the group is statistically significant ($p < 0.05$) compared to the control group which received no incubation with $GNRs@SiO_2@IR780@PEG$.

### 4.2.6 PDT Activity of $GNRs@SiO_2@IR780@PEG$

Firstly, the cells were treated with $GNRs@SiO_2@IR780@PEG$ at a concentration of 10 $\mu$g/mL for 2 hours. After incubation, and washing the cells, the fresh media was added, and a 785 nm laser was used to irradiate cells for 10 minutes at 400 $mW/cm^2$. When data are compared with a control group that received no treatment, the cell viability was 62.7% as shown in Figure 4.20.

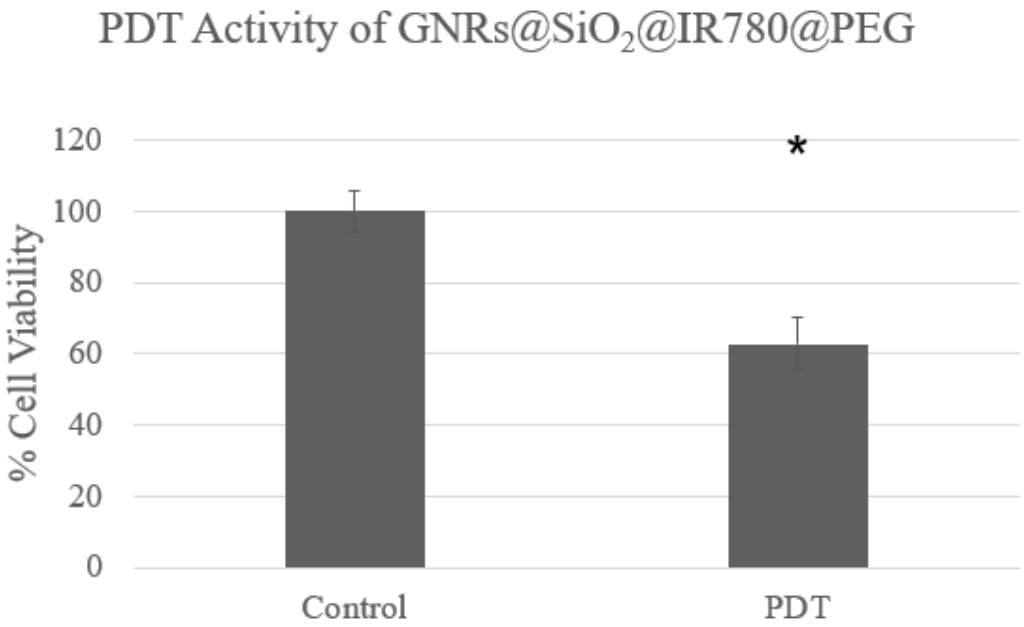


**Figure 4.20** PDT Activity of $GNRs@SiO_2@IR780@PEG$ at a concentration of 10 $\mu$g/mL. We cannot perform the post hoc test in this experiment because we have fewer than three groups. That's why the independent Independent-Samples T-Test analysis was performed. * Shows that the group is statistically significant ($p < 0.05$) compared to the control group which received no incubation with $GNRs@SiO_2@IR780@PEG$.

### 4.2.7 Dark Toxicity of $GNRs@SiO_2@PEG$ and PDT Activity of $GNRs@SiO_2@PEG$

The cells were treated with only $GNRs@SiO_2@PEG$ at a concentration of 10 $\mu$g/mL for 2 hours to compare with only $GNRs@SiO_2@IR780@PEG$ effect on the cells. When data are compared with a control group that had no treatment, the cell viability was 93.8% as shown in Figure 4.21. It can be said that only $GNRs@SiO_2@PEG$ does not show any dark toxicity effect on cancer cells at 10 $\mu$g/mL. After this experiment, the cells were incubated with 10 $\mu$g/mL of $GNRs@SiO_2@PEG$ for 2 hours for the PDT activity experiment. After incubation, and washing the cells, the fresh media was added, and a 785 nm laser was used to expose cells for 10 minutes at 400 $mW/cm^2$. When data are compared with a control group that received no treatment,

the cell viability was 91.51% as shown in Figure 4.22. Thus, we could say that IR780 was very effective for PDT application that provides about 40% cell killing.

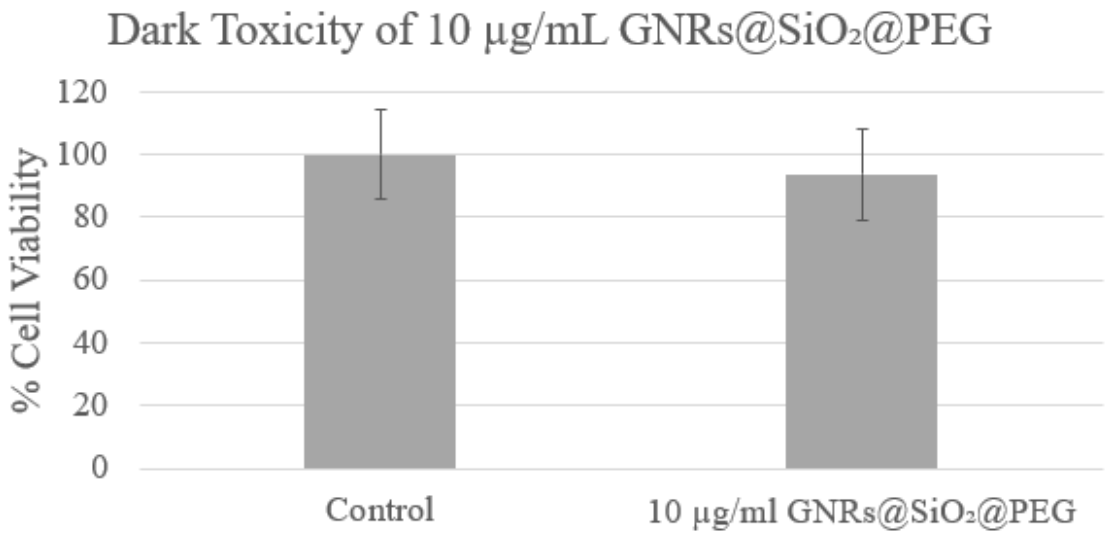


**Figure 4.21** Dark Toxicity of $GNRs@SiO_2@PEG$ at a concentration of 10 $\mu$g/mL.

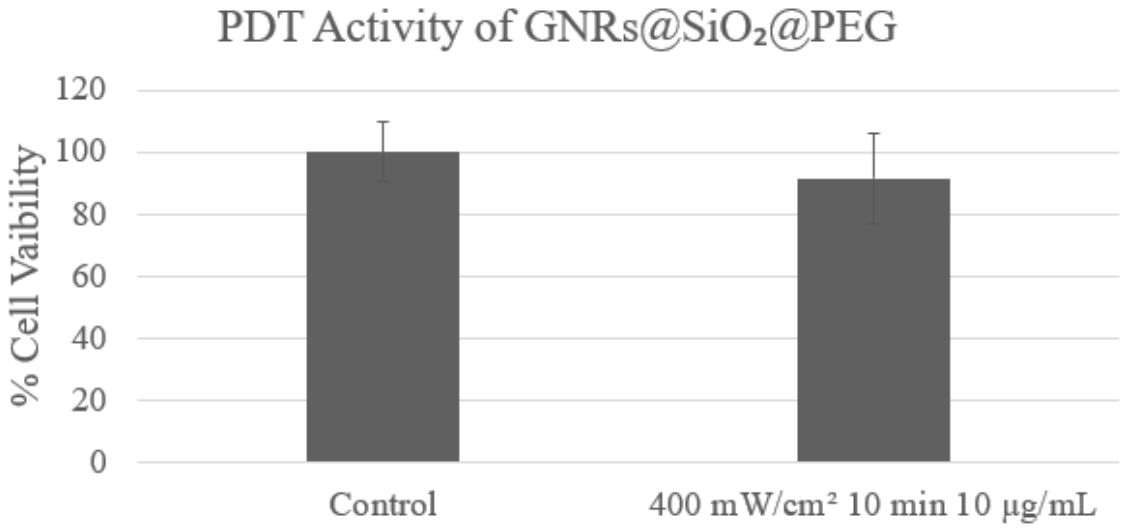


**Figure 4.22** PDT Activity of $GNRs@SiO_2@PEG$ at a concentration of 10 $\mu$g/mL.

### 4.2.8 Comparing All PDT Activities

After obtaining the results, the PDT activities of $GNRs@SiO_2@IR780$, $GNRs@SiO_2@IR780@PEG$, $GNRs@SiO_2$, and $GNRs@SiO_2@PEG$ groups were compared with each other. After comparison, all PDT activities can be seen as statistically different compared to the control group as shown in Figure 4.23.

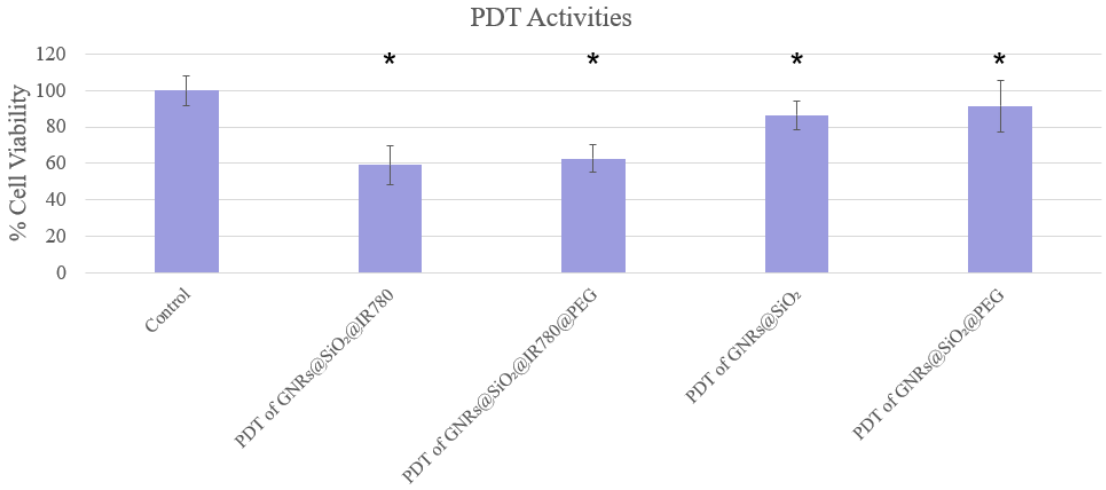


**Figure 4.23** All PDT activities were compared. *Shows that the group is statistically significant ($p < 0.05$) compared to the control group which received no incubation with nanoparticles or laser exposure.

Figure 4.24 shows that there is no significant difference between PDT with $GNRs@SiO_2@IR780$ and PDT with $GNRs@SiO_2@IR780@PEG$. However, PDT groups of $GNRs@SiO_2@IR780$ and $GNRs@SiO_2@IR780@PEG$ are different from PDT with $GNRs@SiO_2$ and $GNRs@SiO_2@PEG$. We can say that the difference is caused by IR780 in these groups. Additionally, there is no significant difference between PDT groups of $GNRs@SiO_2$ and $GNRs@SiO_2@PEG$.

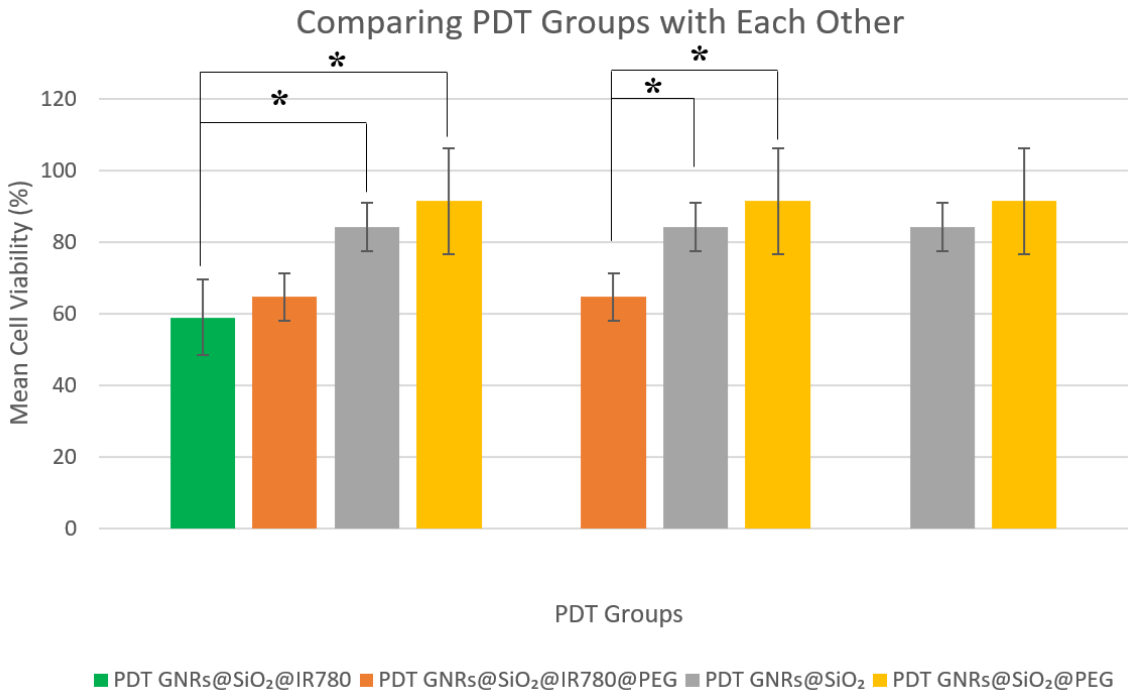


**Figure 4.24** All PDT activities were compared to each other. *Shows that the group is statistically significant ($p < 0.05$) compared to the related group. The Independent-Samples T-Test analysis was performed to compare two groups with each other.

## 4.3 DISCUSSION

In this study, we investigated the PDT efficacy of IR780-loaded silica-coated GNRs on HCT116 colon cancer cells. IR780 is a near-infrared dye that could be used for PDT applications. However, since it is a highly toxic chemical, it should be used as loaded, conjugated, or linked to appropriate nanostructures to overcome its limitations.

Due to utilizing the physical properties of gold nanostructures, we studied gold nanorods that show two absorptions in the visible and NIR region. Their size and shape are attractive for their optical properties, surface functionalization, and drug delivery. In this study, GNRs were coated with mesoporous silica because IR780 could not bind to GNRs directly. Silica coating provides incorporation between GNRs and NIR dye, IR780, so in this way, IR780 can be loaded into the nanostructure.

The loading efficiency of IR780 was calculated with related equations and it was 27.11%. This loading efficiency could not be enough for the effectual PDT results on resistive colon cancer cells. Our future work could be studying the increase of IR780 loading efficiency on $GNRs@SiO_2$ to destroy colon cancer cells efficiently.

Before the experiments with $GNRs@SiO_2@IR780$ to understand the PDT effect, we had to know the only laser effect and only $GNRs@SiO_2$. If we know that, we can see the efficacy of IR780. To see only the laser effect, two different power densities were evaluated with the same energy densities, and we saw that neither experiment showed cell cytotoxicity. Hence, we chose the power density of 400 $mW/cm^2$ and a duration of 10 minutes to obtain the most effective results.

After only laser experiments, the dark toxicity of $GNRs@SiO_2@IR780$ was evaluated at different concentrations to choose one for the PDT applications. After 2 hours of incubation, 2.5 $\mu$g/mL of $GNRs@SiO_2@IR780$ shows no dark toxicity and a significant difference compared with a control group. Therefore, we could use this concentration for PDT applications.

After all, PDT can be applied by using 2.5 $\mu$g/mL $GNRs@SiO_2@IR780$ under 785 nm laser light exposure with 400 $mW/cm^2$ power density and 10 min of application time. The experiment showed a 41% decrease in cell viability. This reduction of cell viability could increase while increasing the loading efficiency of IR780 on $GNRs@SiO_2$.

To show that the cell viability decreased because of IR780 loading and irradiation, the same procedure was applied to $GNRs@SiO_2$. First, the dark toxicity experiment was done by using 2.5 $\mu$g/mL $GNRs@SiO_2$ and after that, the effect of $GNRs@SiO_2$ on the cells was observed under 785 nm laser light exposure with a power density of 400 $mW/cm^2$ and an application duration of 10 min. After the experiment the cell viability was 86.47% as expected, thus we showed the IR780 effect in PDT applications with this comparison.

PDT application by using $GNRs@SiO_2@IR780$ showed 59% cell viability. The

percentage could not be enough to treat HCT116 colon cancer cells. Therefore, after these experiments, we decided to coat the $GNRs@SiO_2@IR780$ with PEG to decrease the cell viability much more. First, the dark toxicity experiment was done by using different concentrations of $GNRs@SiO_2@IR780@PEG$ from 2.5 $\mu$g/mL to 500 $\mu$g/mL and it was chosen to use a concentration of 10 $\mu$g/mL. After that, the effect of $GNRs@SiO_2@IR780@PEG$ on the cells was observed under 785 nm laser light exposure with a power density of 400 $mW/cm^2$ and an application duration of 10 min. The results were not as expected because the cell killing was higher when using $GNRs@SiO_2@IR780@PEG$ compared with $GNRs@SiO_2@IR780$. The cell viability was 62.7% after the experiment and this could be caused by insufficient PEG coating. Another future work could be studying efficient PEG coating, and this could be by using layer by layer method. The process could take place in the following order: synthesis of GNRs, PEG coating of GNRs, silica coating of GNRs, IR780 loading of GNRs, and again PEG coating of GNRs.

To show that the cell viability decreased because of IR780 loading and irradiation, the same procedure was applied to $GNRs@SiO_2@PEG$. First, the dark toxicity experiment was done by using 10 $\mu$g/mL $GNRs@SiO_2@PEG$ and the cell viability was 93.8% which is higher than the dark toxicity of $GNRs@SiO_2$. After that, the effect of $GNRs@SiO_2@PEG$ on the cells was observed under 785 nm laser light exposure with a power density of 400 $mW/cm^2$ and an application duration of 10 min. The cell viability was 91.51% as expected, thus we showed the IR780 effect in PDT applications with this comparison.

The drug loading efficiency is an important factor to obtain effective results from PDT application. We synthesized silica-coated gold nanorods and during GNRs synthesis, the concentration of CTAB is important for the thickness of the silica coating [7]. As mentioned above, our future study could be about increasing IR780 loading efficiency on $GNRs@SiO_2$ and the studying concentration of CTAB would be beneficial during GNRs synthesis. Whether the optimal thickness of silica coating is obtained, IR780 loading efficiency can increase.

PEG coating, PEGylation, provides hydrophilic protective layers around nanostructures and this situation improves the capability of targeted drug delivery, increases the drug loading and drug releases, and provides high nanostructure stability [83–85]. However, it is crucial to adjust the PEG density, and use the correct molecular weight for the optimal PEGylation that affects the physicochemical and biological properties of the nanostructure [83, 86, 87]. As mentioned above, another future work could be about finding the optimal PEGylation procedure on IR780-loaded silica-coated GNRs.

## 4.4 CONCLUSION

In this work, improvement of the effect of PDT with IR780-loaded silica-coated GNRs and PEGylated IR780-loaded silica-coated GNRs on the HCT116 colon cancer cell line was evaluated under 785 nm laser light exposure. The synthesis of GNRs and silica coating were outstanding but the loading efficiency of IR780 to the nanostructure needs to be improved.

The results have shown that phototoxicity of 2.5 $\mu$g/mL $GNRs@SiO_2@IR780$ and 240 $J/cm^2$ dose of energy causes a 41% decrease in cell viability. This percentage of reduction could be improved, and this *in vitro* study shows that $GNRs@SiO_2@IR780$ is a promising nanostructure agent with a 785 nm diode laser for the treatment of the HCT116 colon cancer cells.

Additionally, the results have shown that phototoxicity of 10 $\mu$g/mL $GNRs@SiO_2@IR780@PEG$ and 240 $J/cm^2$ dose of energy causes a 38% reduction in cell viability under 785 nm laser light exposure. This percentage of reduction in cell viability is not enough to destroy the tumor cells as expected and this *in vitro* study needs to be worked on for the treatment of the HCT116 colon cancer cells.

# REFERENCES


1. E. Kukcinaviciute et al. Significance of Notch and Wnt signaling for chemoresistance of colorectal cancer cells HCT116. *Journal of Cellular Biochemistry*, 119(7): 5913–5920, 2018.
2. Y.-S. Chen et al. Enhanced thermal stability of silica-coated gold nanorods for photoacoustic imaging and image-guided therapy. *Optics Express*, 18(9):8867–8878, 2010.
3. E. J. Chung, L. Leon, and C. Rinaldi. *Nanoparticles for Biomedical Applications: Fundamental Concepts, Biological Interactions and Clinical Applications*. Elsevier, 2019, pages 175–193.
4. S. Bhana et al. Photosensitizer-loaded gold nanorods for near infrared photodynamic and photothermal cancer therapy. *Journal of Colloid and Interface Science*, 469:8–16, 2016.
5. H. Abrahamse and M. R. Hamblin. New photosensitizers for photodynamic therapy. *Biochemical Journal*, 473(4):347–364, 2016.
6. C. G. Alves et al. IR780 based nanomaterials for cancer imaging and photothermal, photodynamic and combinatorial therapies. *International Journal of Pharmaceutics*, 542(1-2):164–175, 2018.
7. Z. Zhang et al. Mesoporous silica-coated gold nanorods as a light-mediated multifunctional theranostic platform for cancer treatment. *Advanced Materials*, 24(11): 1418–1423, 2012.
8. T Nagy-Simon et al. IR780-dye loaded gold nanoparticles as new near infrared activatable nanotheranostic agents for simultaneous photodynamic and photothermal therapy and intracellular tracking by surface enhanced resonant raman scattering imaging. *Journal of Colloid and Interface Science*, 517:239–250, 2018.
9. A. S. Gonçalves et al. IR780 loaded gelatin-peg coated gold core silica shell nanorods for cancer-targeted photothermal/photodynamic therapy. *Biotechnology and Bioengineering*, 119(2):644–656, 2022.
10. N. Topaloglu, E. Bakay, M. Yünlü, and G. Onak. Induced photo-cytotoxicity on prostate cancer cells with the photodynamic action of toluidine blue ortho. *Photodiagnosis and Photodynamic Therapy*, 34:102306, 2021.
11. C. J. Gomer. *Photodynamic therapy: methods and protocols*. Springer, 2010.
12. A. P. Castano, T. N. Demidova, and M. R. Hamblin. Mechanisms in photodynamic therapy: part one—photosensitizers, photochemistry and cellular localization. *Photodiagnosis and Photodynamic Therapy*, 1(4):279–293, 2004.
13. S. Siriwibool et al. Near-infrared fluorescent pH responsive probe for targeted photodynamic cancer therapy. *Scientific Reports*, 10(1):1–10, 2020.
14. N. Topaloğlu, G. Kadıköylü, G. Onak, and O. Karaman. The effect of indocyanine green-based photodynamic therapy on healthy fibroblast and keratinocyte cells. *Photodiagnosis and Photodynamic Therapy*, 31:101891, 2020.
15. M. Arruebo et al. Assessment of the evolution of cancer treatment therapies. *Cancers*, 3(3):3279–3330, 2011.

16. J. Coffey et al. Cancer surgery: risks and opportunities. *Bioessays*, 28(4):433–437, 2006.

17. A. Sourati, A. Ameri, and M. Malekzadeh. Acute side effects of radiation therapy. *Cham: Springer*, 2017.

18. M. S. Aslam et al. Side effects of chemotherapy in cancer patients and evaluation of patients opinion about starvation based differential chemotherapy. *Journal of Cancer Therapy*, 2014, 2014.

19. P. Prasad. Wiley interscience (service en ligne) introduction to biophotonics. hoboken, 2004.

20. F. Şueki, M. K. Ruhi, and M. Gülsoy. The effect of curcumin in antitumor photodynamic therapy: In vitro experiments with Caco-2 and PC-3 cancer lines. *Photodiagnosis and Photodynamic Therapy*, 27:95–99, 2019.

21. G. M. F. Calixto et al. Nanotechnology-based drug delivery systems for photodynamic therapy of cancer: a review. *Molecules*, 21(3):342, 2016.

22. Y. I. Svenskaya et al. Photodynamic therapy platform based on localized delivery of photosensitizer by vaterite submicron particles. *Colloids and Surfaces B: Biointerfaces*, 146:171–179, 2016.

23. C. Ji et al. Activatable photodynamic therapy for prostate cancer by NIR dye / photosensitizer loaded albumin nanoparticles. *Journal of Biomedical Nanotechnology*, 15(2):311–318, 2019.

24. D. Şen Karaman et al. Evolving technologies and strategies for combating antibacterial resistance in the advent of the postantibiotic era. *Advanced Functional Materials*, 30(15):1908783, 2020.

25. F. Wu et al. Chlorin e6 and polydopamine modified gold nanoflowers for combined photothermal and photodynamic therapy. *Journal of Materials Chemistry B*, 8(10):2128–2138, 2020.

26. W. Xu et al. A dual-targeted hyaluronic acid-gold nanorod platform with triple-stimuli responsiveness for photodynamic/photothermal therapy of breast cancer. *Acta Biomaterialia*, 83:400–413, 2019.

27. C. Zhang et al. Fluorescence guided photothermal/photodynamic ablation of tumours using pH-responsive chlorin e6-conjugated gold nanorods. *Colloids and Surfaces B: Biointerfaces*, 160:345–354, 2017.

28. H. Li et al. Combination of active targeting, enzyme-triggered release and fluorescent dye into gold nanoclusters for endomicroscopy-guided photothermal / photodynamic therapy to pancreatic ductal adenocarcinoma. *Biomaterials*, 139:30–38, 2017.

29. J. Zeng et al. Porphyrin derivative conjugated with gold nanoparticles for dual-modality photodynamic and photothermal therapies in vitro. *ACS Biomaterials Science & Engineering*, 4(3):963–972, 2018.

30. J. Oh, H. Yoon, and J.-H. Park. Nanoparticle platforms for combined photothermal and photodynamic therapy. *Biomedical Engineering Letters*, 3(2):67–73, 2013.

31. M.-C. Daniel and D. Astruc. Gold nanoparticles: assembly, supramolecular chemistry, quantum-size-related properties, and applications toward biology, catalysis, and nanotechnology. *Chemical Reviews*, 104(1):293–346, 2004.

32. R. Shukla et al. Biocompatibility of gold nanoparticles and their endocytotic fate inside the cellular compartment: a microscopic overview. *Langmuir*, 21(23):10644–10654, 2005.

33. H. S. Kim and D. Y. Lee. Near-Infrared-Responsive cancer photothermal and photodynamic therapy using gold nanoparticles. *Polymers*, 10(9):961, 2018.

34. W. He, G. Ma, Q. Shen, and Z. Tang. Engineering gold nanostructures for cancer treatment: spherical nanoparticles, nanorods, and atomically precise nanoclusters. *Nanomaterials*, 12(10):1738, 2022.

35. N. S. Abadeer and C. J. Murphy. Recent progress in cancer thermal therapy using gold nanoparticles. *The Journal of Physical Chemistry C*, 120(9):4691–4716, 2016.

36. N. Gamaleia et al. Photodynamic activity of hematoporphyrin conjugates with gold nanoparticles: experiments in vitro. *Experimental Oncology*, 32(1):44–47, 2010.

37. H. P. Tham et al. Photosensitizer anchored gold nanorods for targeted combinational photothermal and photodynamic therapy. *Chemical Communications*, 52(57):8854–8857, 2016.

38. H. Xu et al. Effects of light irradiation upon photodynamic therapy based on 5-aminolevulinic acid–gold nanoparticle conjugates in K562 cells via singlet oxygen generation. *International Journal of Nanomedicine*, 7:5029, 2012.

39. R. Chen et al. Near-IR-triggered photothermal/photodynamic dual-modality therapy system via chitosan hybrid nanospheres. *Biomaterials*, 34(33):8314–8322, 2013.

40. J. D. Meyers et al. Peptide-targeted gold nanoparticles for photodynamic therapy of brain cancer. *Particle & Particle Systems Characterization*, 32(4):448–457, 2015.

41. E. Fu, S. A. Ramsey, and P. Yager. Dependence of the signal amplification potential of colloidal gold nanoparticles on resonance wavelength in surface plasmon resonance-based detection. *Analytica Chimica Acta*, 599(1):118–123, 2007.

42. R. Arvizo, R. Bhattacharya, and P. Mukherjee. Gold nanoparticles: opportunities and challenges in nanomedicine. *Expert Opinion on Drug Delivery*, 7(6):753–763, 2010.

43. S.-H. Seo et al. NIR-light-induced surface-enhanced Raman scattering for detection and photothermal/photodynamic therapy of cancer cells using methylene blue-embedded gold nanorod@$SiO_2$ nanocomposites. *Biomaterials*, 35(10):3309–3318, 2014.

44. P. Huang et al. Photosensitizer-conjugated silica-coated gold nanoclusters for fluorescence imaging-guided photodynamic therapy. *Biomaterials*, 34(19):4643–4654, 2013.

45. I. Roy et al. Ceramic-based nanoparticles entrapping water-insoluble photosensitizing anticancer drugs: A novel drug- carrier system for photodynamic therapy. *Journal of the American Chemical Society*, 125(26):7860–7865, 2003.

46. P. Huang et al. Folic acid-conjugated silica-modified gold nanorods for X-RAY/CT imaging-guided dual-mode radiation and photo-thermal therapy. *Biomaterials*, 32(36):9796–9809, 2011.

47. T. Luo et al. Mesoporous silica-coated gold nanorods with embedded indocyanine green for dual mode X-RAY/CT and NIR fluorescence imaging. *Optics Express*, 19(18):17030–17039, 2011.

48. C. Bharti, U. Nagaich, A. K. Pal, and N. Gulati. Mesoporous silica nanoparticles in target drug delivery system: A review. *International Journal of Pharmaceutical investigation*, 5(3):124, 2015.

49. C. Yue et al. IR-780 dye loaded tumor targeting theranostic nanoparticles for NIR imaging and photothermal therapy. *Biomaterials*, 34(28):6853–6861, 2013.

50. K. A. Wilk et al. Photo-oxidative action in MCF-7 cancer cells induced by hydrophobic cyanines loaded in biodegradable microemulsion-templated nanocapsules. *International Journal of Oncology*, 41(1):105–116, 2012.

51. K. Wang et al. Self-assembled IR780-loaded transferrin nanoparticles as an imaging, targeting, and PDT/PTT agent for cancer therapy. *Scientific Reports*, 6(1):1–11, 2016.

52. Y. Zhan et al. Silica cross-linked micellar core–shell nanoparticles encapsulating IR-780 with strong bright and good biocompatibility for optical imaging in vivo. *Journal of Biomedical Nanotechnology*, 13(2):144–154, 2017.

53. A. S. Gonçalves et al. IR780 loaded gelatin-PEG coated gold core silica shell nanorods for cancer-targeted photothermal/photodynamic therapy. *Biotechnology and Bioengineering*, 119(2):644–656, 2022.

54. F. Xia et al. Matrix metallopeptidase 2 targeted delivery of gold nanostars decorated with IR-780 iodide for dual-modal imaging and enhanced photothermal/ photodynamic therapy. *Acta Biomaterialia*, 89:289–299, 2019.

55. C. Jiang et al. Hydrophobic IR780 encapsulated in biodegradable human serum albumin nanoparticles for photothermal and photodynamic therapy. *Acta Biomaterialia*, 14:61–69, 2015.

56. M. G. C. Machado et al. Photodynamic therapy with the dual-mode association of IR780 to PEG-PLA nanocapsules and the effects on human breast cancer cells. *Biomedicine & Pharmacotherapy*, 145:112464, 2022.

57. H. Li et al. Dual-function nanostructured lipid carriers to deliver IR780 for breast cancer treatment: Anti-metastatic and photothermal anti-tumor therapy. *Acta Biomaterialia*, 53:399–413, 2017.

58. J. Li et al. Near-infrared-induced IR780-loaded PLGA nanoparticles for photothermal therapy to treat breast cancer metastasis in bones. *RSC Advances*, 9(62):35976–35983, 2019.

59. P. Rawla, T. Sunkara, and A. Barsouk. Epidemiology of colorectal cancer: incidence, mortality, survival, and risk factors. *Gastroenterology Review/Przegląd Gastroenterologiczny*, 14(2):89–103, 2019.

60. A. Rajput et al. Characterization of HCT116 human colon cancer cells in an orthotopic model. *Journal of Surgical Research*, 147(2):276–281, 2008.

61. P. S. Steeg. Metastasis suppressors alter the signal transduction of cancer cells. *Nature Reviews Cancer*, 3(1):55–63, 2003.

62. T. A. Martin et al. Cancer invasion and metastasis: molecular and cellular perspective. In *Madame Curie Bioscience Database [Internet]*. Landes Bioscience, 2013.

63. I. J. Fidler. Critical determinants of metastasis. In *Seminars in Cancer Biology*, volume 12, pages 89–96. Elsevier, 2002.

64. Y. Ma et al. $H_2S$-activable MOF nanoparticle photosensitizer for effective photodynamic therapy against cancer with controllable singlet-oxygen release. *Angewandte Chemie*, 129(44):13940–13944, 2017.

65. M. Tanaka et al. Anticancer effects of novel photodynamic therapy with glycoconjugated chlorin for gastric and colon cancer. *Anticancer Research*, 31(3):763–769, 2011.

66. B. Chu et al. ROS-responsive camptothecin prodrug nanoparticles for on-demand drug release and combination of chemotherapy and photodynamic therapy. *Advanced Functional Materials*, 30(52):2005918, 2020.

67. M. Ballestri et al. Core–shell poly-methyl methacrylate nanoparticles covalently functionalized with a non-symmetric porphyrin for anticancer photodynamic therapy. *Journal of Photochemistry and Photobiology B: Biology*, 186:169–177, 2018.

68. B. Nikoobakht and M. A. El-Sayed. Preparation and growth mechanism of gold nanorods (NRs) using seed-mediated growth method. *Chemistry of Materials*, 15(10):
1957–1962, 2003.

69. Z. C. Canbek. *Influence de taille et de la structure des germes dans la formation de nanoparticules d'or* A*nisotropes*. PhD thesis, Versailles-St Quentin en Yvelines, 2014.

70. I. Gorelikov and N. Matsuura. Single-step coating of mesoporous silica on cetyltrimethyl ammonium bromide-capped nanoparticles. *Nano Letters*, 8(1):369–373, 2008.

71. Y.-S. Lin and C. L. Haynes. Synthesis and characterization of biocompatible and size-tunable multifunctional porous silica nanoparticles. *Chemistry of Materials*, 21(17):3979–3986, 2009.

72. A. Schroeder et al. Treating metastatic cancer with nanotechnology. *Nature Reviews Cancer*, 12(1):39–50, 2012.

73. W.-C. Wu and J. B. Tracy. Large-scale silica overcoating of gold nanorods with tunable shell thicknesses. *Chemistry of Materials*, 27(8):2888–2894, 2015.

74. C. O. Silva et al. Current trends in cancer nanotheranostics: metallic, polymeric, and lipid-based systems. *Pharmaceutics*, 11(1):22, 2019.

75. Z. Hussain et al. Nanomedicines as emerging platform for simultaneous delivery of cancer therapeutics: new developments in overcoming drug resistance and optimizing anticancer efficacy. *Artificial Cells, Nanomedicine, and Biotechnology*, 46(sup2):1015–1024, 2018.

76. B. Güleryüz. *Photodynamic Therapy with Upconversion Nanoparticles*. PhD thesis, Bogazici University, 2022.

77. M. Güney Akkurt. *Indocyanine Green Loaded Poly(Lactic Acid) Nanoparticles Mediated Phototherapy of Cancer*. PhD thesis, Bogazici University, 2022.

78. F. Hubert, F. Testard, and O. Spalla. Cetyltrimethylammonium bromide silver bromide complex as the capping agent of gold nanorods. *Langmuir*, 24(17):9219–9222, 2008.

79. A. Gole and C. J. Murphy. Seed-mediated synthesis of gold nanorods: role of the size and nature of the seed. *Chemistry of Materials*, 16(19):3633–3640, 2004.

80. S. Köppl. *Seed-mediated synthesis of high aspect ratio nanorods and nanowires of gold and silver*. PhD thesis, ETH Zurich, 2011.

81. R. M. Silverstein and G. C. Bassler. Spectrometric identification of organic compounds. *Journal of Chemical Education*, 39(11):546, 1962.

82. D. Lee, R. Condrate, and W. Lacourse. FTIR spectral characterization of thin film coatings of oleic acid on glasses Part II coatings on glass from different media such as water, alcohol, benzene and air. *Journal of Materials Science*, 35(19):4961–4970, 2000.

83. L. Shi et al. Effects of polyethylene glycol on the surface of nanoparticles for targeted drug delivery. *Nanoscale*, 13(24):10748–10764, 2021.

84. T. U. Wani, S. N. Raza, and N. A. Khan. Nanoparticle opsonization: Forces involved and protection by long chain polymers. *Polymer Bulletin*, 77(7):3865–3889, 2020.

85. Kenry et al. Mechanistic understanding of the biological responses to polymeric nanoparticles. *ACS Nano*, 14(4):4509–4522, 2020.

86. C. Sanchez-Cano and M. Carril. Recent developments in the design of non-biofouling coatings for nanoparticles and surfaces. *International Journal of Molecular Sciences*, 21(3):1007, 2020.

87. S. Y. Fam et al. Stealth coating of nanoparticles in drug-delivery systems. *Nanomaterials*, 10(4):787, 2020.